

GigaScience

Conventional and hyperspectral time-series imaging of maize lines widely used in field trials

--Manuscript Draft--

| | | |
|--|---|----------------------|
| Manuscript Number: | GIGA-D-17-00187R2 | |
| Full Title: | Conventional and hyperspectral time-series imaging of maize lines widely used in field trials | |
| Article Type: | Data Note | |
| Funding Information: | Nebraska Corn Board (88-R-1617-03) | Dr. James C Schnable |
| | Iowa Corn Board | Dr. James C Schnable |
| | National Science Foundation (OIA-1557417) | Dr. James C Schnable |
| Abstract: | <p>Background: Maize (<i>Zea mays</i> ssp. <i>mays</i>) is one of three crops, along with rice and wheat, responsible for more than 1/2 of all calories consumed around the world. Increasing the yield and stress tolerance of these crops is essential to meet the growing need for food. The cost and speed of plant phenotyping is currently the largest constraint on plant breeding efforts. Datasets linking new types of high throughput phenotyping data collected from plants to the performance of the same genotypes under agronomic conditions across a wide range of environments are essential for developing new statistical approaches and computer vision based tools.</p> <p>Findings: A set of maize inbreds - primarily recently off patent lines -- were phenotyped using a high throughput platform at University of Nebraska-Lincoln. These lines have been previously subjected to high density genotyping, and scored for a core set of 13 phenotypes in field trials across 13 North American states in two years by the Genomes to Fields consortium. A total of 485 GB of image data including RGB, hyperspectral, fluorescence and thermal infrared photos has been released.</p> <p>Conclusions: Correlations between image-based measurements and manual measurements demonstrated the feasibility of quantifying variation in plant architecture using image data. However, naive approaches to measuring traits such as biomass can introduce nonrandom measurement errors confounded with genotype variation. Analysis of hyperspectral image data demonstrated unique signatures from stem tissue. Integrating heritable phenotypes from high-throughput phenotyping data with field data from different environments can reveal previously unknown factors influencing yield plasticity.</p> | |
| Corresponding Author: | James Schnable University of Nebraska-Lincoln Lincoln, NE UNITED STATES | |
| Corresponding Author Secondary Information: | | |
| Corresponding Author's Institution: | University of Nebraska-Lincoln | |
| Corresponding Author's Secondary Institution: | | |
| First Author: | Zhikai Liang | |
| First Author Secondary Information: | | |
| Order of Authors: | Zhikai Liang | |
| | Piyush Pandey | |
| | Vincent Stoerger | |
| | Yuhang Xu | |
| | Yumou Qiu | |
| | Yufeng Ge | |

James C Schnable

Order of Authors Secondary Information:

Response to Reviewers:

I am pleased to inform you that it is potentially acceptable for publication in GigaScience, once you have carried out some final minor essential revisions.

1) Please see the attached PDF with marked up comments which need to be addressed.- note URLs must be moved to the references and only the reference number cited in the main text.

Response: We have moved each URL to references rather than embedding them in text.

2) Please fix this URL which is currently broken:
<http://cbsusrv04.tc.cornell.edu/users/panzea/download.aspx?%1Flegroupid=4>

Response: We have replaced this link with one to a more general portion of the website which is less likely to stop working, and provided a reference ID readers can use to find the specific dataset we downloaded.

3) once you have made our marked up final edits, please submit a clean version online. Note that we will need all Latex source files PLUS a Word.docx version of the manuscript.

Response: We have made the edited requested in the marked up PDF. We are uploading all LaTeX source files, plus a docx file which we have reviewed to be as close to the original LaTeX as possible (but in the case of any discrepancy between the two, please treat the LaTeX as the ground truth). Note that we had to make one edit to the bst file provided in the GigaScience on Overleaf, as the default bst file was numbering references alphabetically by author's last name, and looking at other papers published in GigaScience it appears the correct style is to number references based on their order of appearance in the manuscript.

Reviewer reports:

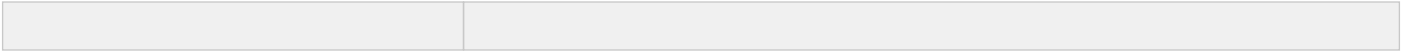
Reviewer #2: This manuscript describes the generation of a time-series dataset of conventional and hyperspectral images of commonly known and important maize lines. The authors describe the methods of data collection and how it is useful, especially in conjunction with other already available datasets for the same lines. The authors begin to analyze the dataset generated, focusing on biomass measures and determining heritability. The authors conclude that they believe it is important and necessary to combine controlled environment data with field data to tackle problems facing crop production.

Comments:

I want to clarify my first review of this manuscript. It was not my intention to make it seem as the dataset generated for this manuscript is not important, large, or useful for the broader maize and plant phenotyping community. This dataset could be very useful for some research groups, including the corresponding authors group. The authors response to the age question of the dataset of, look at the cycle time of data collection to publication in plant phenomics is generally longer, I totally agree with. The authors give numerous examples to back up this point. I'm not disputing this, but the authors should also note the amount of downstream analyses and new biological findings that are in these manuscripts as well. The importance of the presented dataset as outlined by the authors is its ability to link with other already available datasets, which isn't shown in the manuscript. This paper is a data release paper with a valuable, controlled, and well documented dataset. The real value in the dataset will be shown in subsequent publications that begin to combine the multiple datasets available from these maize lines (field phenotyping, genotyping, controlled environment phenotyping).

Response: We are in complete agreement with the reviewer that the real scientific value of this data release will come from downstream analyses and biological insights conducted using the dataset and other other associated datasets from the same maize lines. This manuscript does not include significant new biological findings of our own, it

| | |
|---|--|
| | is only an attempt to get our raw data out in a form that other researchers can also use it without waiting the additional 1-3 years it would take (if the timelines of prior plant phenotypic papers are a useful guide) for us to tell our own biological story with this dataset. |
| Additional Information: | |
| Question | Response |
| Are you submitting this manuscript to a special series or article collection? | No |
| Experimental design and statistics | Yes |
| <p>Full details of the experimental design and statistical methods used should be given in the Methods section, as detailed in our Minimum Standards Reporting Checklist. Information essential to interpreting the data presented should be made available in the figure legends.</p> <p>Have you included all the information requested in your manuscript?</p> | |
| Resources | Yes |
| <p>A description of all resources used, including antibodies, cell lines, animals and software tools, with enough information to allow them to be uniquely identified, should be included in the Methods section. Authors are strongly encouraged to cite Research Resource Identifiers (RRIDs) for antibodies, model organisms and tools, where possible.</p> <p>Have you included the information requested as detailed in our Minimum Standards Reporting Checklist?</p> | |
| Availability of data and materials | Yes |
| <p>All datasets and code on which the conclusions of the paper rely must be either included in your submission or deposited in publicly available repositories (where available and ethically appropriate), referencing such data using a unique identifier in the references and in the “Availability of Data and Materials” section of your manuscript.</p> <p>Have you have met the above requirement as detailed in our Minimum Standards Reporting Checklist?</p> | |





GigaScience, 2017, 1–10

doi: xx.xxxx/xxxx

Manuscript in Preparation
Data Notes

DATA NOTES

Conventional and hyperspectral time-series imaging of maize lines widely used in field trials

Zhikai Liang¹, Piyush Pandey², Vincent Stoerger³, Yuhang Xu⁴, Yumou Qiu⁴, Yufeng Ge² and James C. Schnable^{1,*}

¹Center for Plant Science Innovation, Department of Agronomy and Horticulture, University of Nebraska–Lincoln, Lincoln, 68503, USA and ²Department of Biological System Engineering, University of Nebraska–Lincoln, Lincoln, 68503, USA and ³Plant Phenotyping Facilities Manager, University of Nebraska–Lincoln, Lincoln, 68503, USA and ⁴Department of Statistics, University of Nebraska–Lincoln, Lincoln, 68503, USA

*schnable@unl.edu

Abstract

Background: Maize (*Zea mays* ssp. *mays*) is one of three crops, along with rice and wheat, responsible for more than 1/2 of all calories consumed around the world. Increasing the yield and stress tolerance of these crops is essential to meet the growing need for food. The cost and speed of plant phenotyping is currently the largest constraint on plant breeding efforts. Datasets linking new types of high throughput phenotyping data collected from plants to the performance of the same genotypes under agronomic conditions across a wide range of environments are essential for developing new statistical approaches and computer vision based tools.

Findings: A set of maize inbreds – primarily recently off patent lines – were phenotyped using a high throughput platform at University of Nebraska–Lincoln. These lines have been previously subjected to high density genotyping, and scored for a core set of 13 phenotypes in field trials across 13 North American states in two years by the Genomes 2 Fields consortium. A total of 485 GB of image data including RGB, hyperspectral, fluorescence and thermal infrared photos has been released.

Conclusions: Correlations between image-based measurements and manual measurements demonstrated the feasibility of quantifying variation in plant architecture using image data. However, naive approaches to measuring traits such as biomass can introduce nonrandom measurement errors confounded with genotype variation. Analysis of hyperspectral image data demonstrated unique signatures from stem tissue. Integrating heritable phenotypes from high-throughput phenotyping data with field data from different environments can reveal previously unknown factors influencing yield plasticity.

Key words: Maize; Image; Phenomics; Field-phenotype

Data Description

Background

The green revolution created a significant increase in the yields of several major crops in the 1960s and 1970s, dramatically reducing the prevalence of hunger and famine around the world, even as population growth continued. One of the major com-

ponents of the green revolution was new varieties of major grain crops produced through conventional phenotypic selection with higher yield potentially. Since the green revolution, the need for food has continued to increase, and a great deal of effort in the public and private sectors is devoted to developing crop varieties with higher yield potential. However, as the low hanging fruit for increased yield vanish, each new increase in yield requires more time and resources. Recent studies have

Compiled on: November 7, 2017.

Draft manuscript prepared by the author.

demonstrated that yield increases may have slowed or stopped for some major grain crops in large regions of the world [1]. New approaches to plant breeding must be developed if crop production continues to grow to meet the needs of an increasing population around the world.

The major bottleneck in modern plant breeding is phenotyping. Phenotyping can be used in two ways. Firstly, by phenotyping a large set of lines, a plant breeder can identify those lines with the highest yield potential and/or greatest stress tolerance in a given environment. Secondly, sufficiently detailed phenotyping measurements from enough different plants can be combined with genotypic data to identify regions of the genome of a particular plant species which carry beneficial or deleterious alleles. The breeder can then develop new crop varieties which incorporate as many beneficial alleles and exclude as many deleterious alleles as possible. Phenotyping tends to be expensive and low throughput, yet as breeders seek to identify larger numbers of alleles each with individually smaller effects, the amount of phenotyping required to achieve a given increase in yield potential is growing. High throughput computer vision based approaches to plant phenotyping have the potential to ameliorate this bottleneck. These tools can be used to precisely quantify even subtle traits in plants and will tend to decrease in unit cost with scale, while conventional phenotyping, which remains a human labor intensive processes, does not.

Several recent pilot studies have applied a range of image-processing techniques to extract phenotypic measurements from crop plants. RGB (R: Red channel; G: Green channel; B: Blue channel) camera technology, widely used in the consumer sector, has also been the most widely used tool in these initial efforts at computer vision based plant phenotyping [2, 3, 4, 5]. Other types of cameras including fluorescence [6, 7] and NIR (near-infrared) [6, 8, 9] have also been employed in high throughput plant phenotyping efforts, primarily in studies of the response of plant to different abiotic stresses.

However, the utility of current studies is limited in two ways. Firstly, current analysis tools can extract only a small number of different phenotypic measurements from images of crop plants. Approximately 150 tools for analyzing plant image data are listed in a field specific database, however the majority of these are either developed specifically for *Arabidopsis thaliana* which is a model plant, or are designed specifically to analyze images of roots [10]. Secondly, a great deal of image data is generated in controlled environments, however, there are comparatively few attempts to link phenotypic measurements in the greenhouse to performance in the field. However, one recent report in maize suggested that more than 50% of the total variation in yield under field conditions could be predicted using traits measured under controlled environments [5].

Advances in computational tools for extracting phenotypic measurements of plants from image data and statistical models for predicting yield under different field conditions from such measurements requires suitable training datasets. Here, we generate and validate such a dataset consisting of high throughput phenotyping data from 32 distinct maize (*Zea mays*) accessions drawn primarily from recently off-patent lines developed by major plant breeding companies. These accessions were selected specifically because paired data from the same lines exists for a wide range of plant phenotypes collected in 54 distinct field trials at locations spanning 13 North American states or provinces over two years [11]. This extremely broad set of field sites captures much of the environmental variation among areas in which maize are cultivated with total rainfall during the growing season ranging from 133.604 mm to 960.628 mm (excluding sites with supplemental irrigation) and peak temperatures during the growing season ranging from 23.5°C to 34.9°C. In addition, the same lines have

been genotyped for approximately 200,000 SNP markers using GBS [11]. Towards these existing data, we added RGB, thermal infra-red, fluorescent and hyperspectral images collected once per day per plant, as well as detailed water-use information (single day, single plant resolution). At the end of the experiment, 12 different types of ground-truth phenotypes were measured for individual plants including destructive measurements. A second experiment focused on interactions between genotype and environmental stress, collecting the same types of data described above from two maize genotypes under well watered and water stressed conditions [12]. We are releasing this curated dataset of high throughput plant phenotyping images from accessions where data on both genotypic variation and agronomic performance under field conditions is already available. All data was generated using a Lemnatec designed high throughput greenhouse-based phenotyping system constructed at the University of Nebraska-Lincoln. This system is distinguished from existing public sector phenotyping systems in North America by both the ability to grow plants to a height of 2.5 meters and the incorporation of a hyperspectral camera [9]. Given the unique properties described above, this comprehensive data set should lower the barriers to the development of new computer vision approaches or statistical methodologies by independent researchers who do not have the funding or infrastructure to generate the wide range of different types of data needed.

Methods

Greenhouse Management

All imaged plants were grown in the greenhouse facility of the University of Nebraska-Lincoln's Greenhouse Innovation Center (Latitude: 40.83, Longitude: -96.69) between October 2nd, 2015 to November 10th, 2015. Kernels were sown in 1.5 gallon pots with Fafard germination mix supplemented with 1 cup (236 mL) of Osmocote plus 15-9-12 and one tablespoon (15 mL) of Micromax Micronutrients per 2.8 cubic feet (80 L) of soil. The target photoperiod was 14:10 with supplementary light provided by LED growth lamps from 07:00 to 21:00 each day. The target temperature of the growth facility was between 24 - 26°C. Pots were weighed once per day and watered back to a target weight of 5,400 grams from 10-09-2015 to 11-07-2015 and a target weight of 5,500 grams from 11-08-2015 to the termination of the experiment.

Experimental Design

A total of 156 plants, representing the 32 genotypes listed in Table 1 were grown and imaged, as well as 4 pots with soil but no plant which serve as controls for the amount of water lost from soil as a result of non-transpiration mechanisms (e.g. evaporation). The 156 plants plus control pots were arranged in a ten row by sixteen column grid, with 0.235 meter spacing between plants in the same row and 1.5 meters spacing between rows (Table 2). Sequential pairs of two rows were consisted of a complete replicate with either 31 genotypes and one empty control pot, or 32 genotypes. Within each pair of rows, genotypes were blocked in groups of eight (one half row), with order randomized within blocks between replicates in order to maximize statistical power to analyze within-greenhouse variation.

Plant Imaging

The plants were imaged daily using four different cameras in separate imaging chambers. The four types of cameras were thermal infrared, fluorescence, conventional RGB, and hyperspectral [12]. Images were collected in the order that the camera types are listed in the previous sentence. On each day, plants were imaged sequentially by row, starting with row 1

Table 1. 32 genotypes in maize phenotype map

| Genotype ID | Genotype | Source | Released Year |
|-------------|----------|---------------------|---------------|
| ZL1 | 740 | Novartis Seeds | 1998 |
| ZL2 | 2369 | Cargill | 1989 |
| ZL3 | A619 | Public Sector | 1992 |
| ZL4 | A632 | Public Sector | 1992 |
| ZL5 | A634 | Public Sector | 1992 |
| ZL6 | B14 | Public Sector | 1968 |
| ZL7 | B37 | Public Sector | 1971 |
| ZL8 | B73 | Public Sector | 1972 |
| ZL9 | C103 | Public Sector | 1991 |
| ZL10 | CM105 | Public Sector | 1992 |
| ZL11 | LH123HT | Holden's Foundation | 1984 |
| ZL12 | LH145 | Holden's Foundation | 1983 |
| ZL13 | LH162 | Holden's Foundation | 1990 |
| ZL14 | LH195 | Holden's Foundation | 1989 |
| ZL15 | LH198 | Holden's Foundation | 1991 |
| ZL16 | LH74 | Holden's Foundation | 1983 |
| ZL17 | LH82 | Holden's Foundation | 1985 |
| ZL18 | Mo17 | Public Sector | 1964 |
| ZL19* | DKPB80 | DEKALB Genetics | ? |
| ZL20 | PH207 | Pioneer Hi-Bred | 1983 |
| ZL21 | PHB47 | Pioneer Hi-Bred | 1983 |
| ZL22** | PHG35 | Pioneer Hi-Bred | 1983 |
| ZL23 | PHG39 | Pioneer Hi-Bred | 1983 |
| ZL24 | PHG47 | Pioneer Hi-Bred | 1986 |
| ZL25 | PHG83 | Pioneer Hi-Bred | 1985 |
| ZL26 | PHJ40 | Pioneer Hi-Bred | 1986 |
| ZL27 | PHN82 | Pioneer Hi-Bred | 1989 |
| ZL28 | PHV63 | Pioneer Hi-Bred | 1988 |
| ZL29 | PHW52 | Pioneer Hi-Bred | 1988 |
| ZL30 | PHZ51 | Pioneer Hi-Bred | 1986 |
| ZL31 | W117HT | Public Sector | 1982 |
| ZL32 | Wf9 | Public Sector | 1991 |

* Not currently available for order.

** Genotype represented by only a single plant in the dataset.

column 1 and concluding with row 10, column 16 (Table 2).

Plants were imaged from the side at two angles offset 90 degrees from each other as well as a top down view. On the first day of imaging or when plants reached the two leaf stage of development, the pot was rotated so that the major axis of leaf phylotaxy was parallel to the camera in the PA0 orientation and perpendicular to the camera in the PA90 orientation. This orientation is consistent for all cameras and was not adjusted again for the remainder of the experiment. The fluorescence camera captured images with a resolution of 1038×1390 pixels and measures emission intensity at wavelengths between 500–750 nm based on excitation with light at 400–500 nm. Plants were imaged using the same three perspectives employed for the thermal infrared camera. The RGB camera captured images with a resolution of 2454×2056 pixels. Initially the zoom of the RGB camera in side views was set such that each pixel corresponds to 0.746 mm at the distance of the pot from the camera. Between 2015–11–05 and 2015–11–10, the zoom level of the RGB camera was reduced to keep the entire plant in the frame of the image. As a result of a system error, this same decreased zoom level was also applied to all RGB images taken on 2015–10–20. At this reduced zoom level, each pixel corresponds to 1.507 mm at the distance of the pot from the camera, an approximate 2x change. Plants were also imaged using the same three perspectives employed for the thermal infrared camera. The hyperspectral camera captured images with a resolution of 320 horizontal pixels. As a result of the scanning technology employed, vertical resolution ranged from 494 to 499 pixels. Hyperspectral imaging was conducted using illumination from halogen bulbs (Manufacturer Sylvania, model # ES50 HM UK

240V 35W 25° GU10). A total of 243 separate intensity values were captured for each pixel spanning a range of light wavelengths between 546nm–1700nm. Data from each wavelength was stored as a separate grayscale image.

Ground Truth Measurement

Ground truth measurements were collected at the termination of data collection on November 11–12, 2015. Manually collected phenotypes included plant height, total number of visible leaves, number of total fully extended leaves, stem diameter at the base of the plant, stem diameter at the collar of the top fully extended leaf, length and width of top fully extended leaf, and presence/absence visible anthocyanin production in the stem. After these measurements, total above-ground fresh weight biomass was measured for four out of five replicates, resulting in the destruction of the plants. Ground truth data for the drought stressed subset of this dataset was collected following the procedure previously described in [12].

RGB Image Processing

Pixels covering portions of the plant were segmented out of RGB images using a green index $((2 \times G)/(R+B))$. Pixels with an index value greater than 1.15 [12] were considered to be plant pixels. This method produced some false positive plant pixels within the reflective metal columns at the edge of the image. To reduce the impact of false positives, these areas were excluded from the analysis. Therefore, when plant leaves cross the reflective metal frame, some true plant pixels were excluded. If no plant pixels were identified in the image – often the case in the first several days when the plant had either not germinated or had not risen above the edge of the pot – the value was recorded as "NA" in the output file.

Heritability Analysis

A linear regression model was used to analyze the genotype effect (excluding genotype ZL22 which lacked replication) and greenhouse position effect on plant traits. The responses were modeled independently for each day as

$$y_{h,ij,t} = \mu_{h,t} + \alpha_{h,i,t} + \gamma_{h,\nu(i,j),t} + \epsilon_{h,ij,t}, \quad (1)$$

where the subscript $h = 1, \dots, 6$ denotes the three responses extracted from the images: plant height, width and size for the two views 0 and 90 degree. The subscripts i, j and t denote the j th plant in the i th row and day t , respectively, and $\nu(i, j)$ stands for the genotype at this pot. The parameters α and γ denote row effect and genotype effect, respectively. The error term is $\epsilon_{h,ij,t}$. Let $SS_{\alpha,t}$, $SS_{\gamma,t}$ and $SS_{\epsilon,t}$ be the sum of squares of the regression model (1) for the row effect, genotype effect and the error at time t , respectively. Let $SS_t = SS_{\alpha,t} + SS_{\gamma,t} + SS_{\epsilon,t}$ be the total sum of squares at time t . The heritability HR_t (2) of a given trait within this population was defined as the ratio of the genotype sum of squares over the sum of genotype and error sum of squares. For the estimate of the heritability of measurement error, the row effect term was replaced by a replicate effect (each replicate consisted of two sequential rows) with exclusion of ZL22 as only one plant of this genotype was grown.

$$HR_t = \frac{SS_{\gamma,t}}{SS_{\epsilon,t} + SS_{\gamma,t}}. \quad (2)$$

As the heritability index may change over the growth of the plant, a nonparametric smoothing method was provided for analyzing the time varying heritability of plants. The definition in (3) excludes the variation brought by the greenhouse row effect, which can be considered as the percentage of the variation

Table 2. Experimental layout (ID: ZL1-ZL32). At the time this experiment was conducted, the total size of the UNL greenhouse system was ten rows by twenty columns. Positions marked with UP indicate pots filled with plants from an unrelated experiment, while positions marked with NA indicate pots which had no plants. The first complete replicate is shown in color, and the four incomplete blocks within the first replicate are marked in different colors. * marks empty pots within the experimental design.

| | | | | | | | | | | | | | | | | | | | |
|----|----|----|----|----|----|----|----|----|----|----|----|----|----|----|----|----|----|----|----|
| 9 | 7 | 3 | 10 | 23 | 25 | 26 | 19 | 13 | 5 | 29 | 21 | 2 | 4 | 18 | 20 | UP | UP | UP | UP |
| 11 | 16 | 1 | 32 | 17 | 27 | 6 | 22 | 24 | 31 | 14 | 30 | 15 | 28 | 8 | 12 | UP | UP | UP | UP |
| 29 | 31 | 15 | 13 | 1 | 17 | 25 | 9 | 21 | 30 | 3 | 5 | * | 19 | 14 | 6 | UP | UP | UP | UP |
| 12 | 23 | 32 | 16 | 7 | 28 | 2 | 18 | 10 | 11 | 8 | 26 | 27 | 4 | 20 | 24 | UP | UP | UP | UP |
| 25 | 9 | 21 | 27 | 28 | 12 | 5 | 11 | 15 | 6 | * | 7 | 4 | 23 | 31 | 20 | UP | UP | UP | UP |
| 19 | 32 | 29 | 24 | 16 | 13 | 3 | 8 | 17 | 14 | 18 | 30 | 10 | 26 | 1 | 2 | UP | UP | UP | UP |
| 8 | 1 | 17 | 23 | 21 | 5 | 7 | 24 | 27 | 18 | 3 | 11 | 31 | 15 | 19 | 2 | NA | NA | NA | NA |
| 25 | 30 | 4 | 9 | 16 | 32 | 14 | 20 | * | 10 | 6 | 29 | 28 | 12 | 26 | 13 | NA | NA | NA | NA |
| 15 | 10 | 5 | 32 | 31 | 21 | 16 | 26 | 2 | 18 | 9 | 25 | 6 | 8 | 24 | * | NA | NA | NA | NA |
| 29 | 13 | 23 | 14 | 27 | 7 | 11 | 30 | 12 | 1 | 28 | 4 | 3 | 20 | 17 | 19 | NA | NA | NA | NA |

in plant response that can be explained by the genotype effect after adjusting the environmental effect. To compare with this definition of heritability (2), the response in the model without considering the row effect was constructed as

$$y_{h,ij,t} = \mu_{h,t} + \gamma_{h,\nu(i,j),t} + \epsilon_{h,ij,t} \quad (3)$$

where similarly as (1), $\nu(i, j)$ is the genotype of the j th plant in the i th row. Let $\tilde{SS}_{\gamma,t}$ and \tilde{SS}_t be the genotype sum of squares and total sum of squares under (4). The classical heritability is defined as

$$\tilde{HR}_t = \frac{\tilde{SS}_{\gamma,t}}{\tilde{SS}_t} \quad (4)$$

Hyperspectral Image Processing

Two methods and thresholds were used to extract plant regions of interest from hyperspectral images. First, the commonly used NDVI (normalized difference vegetation index) formula was applied to all pixels using the formula $(R_{750nm} - R_{705nm}) / (R_{750nm} + R_{705nm})$, and pixels with a value greater than 0.25 were classified as originating from the plant [13]. Second, based on the difference in reflectance between stem and leaves at wavelengths of 1056nm and 1151nm, the stem was segmented from other part of plants by selecting pixels where $(R_{1056nm} / R_{1151nm})$ produced a value greater than 1.2. Leaf pixels were defined as pixels identified as plant pixels based on NDVI but not classified as stem pixels. In addition to the biological variation between individual plants, overall intensity variation existed both between different plants imaged on the same day and the same plant on different days as a result of changes in the performance of the lighting used in the hyperspectral imaging chamber. To calibrate each individual image and make the results comparable, a python script (hosted on Github; see code availability section) was used to normalize the intensity values of each plant pixel using data from the non-plant pixels in the same image.

In order to visualize variation across 243 separate wavelength measurements across multiple plant images, we used a PCA (Principal Component Analysis) based approach. After the normalization described above, PCA analysis of intensity values for individual pixels was conducted. PCA values of each individual plant pixel per analyzed plant were translated to intensity values using the formula $[x - \min(x)] / [\max(x) - \min(x)]$. False color RGB images were constructed with the values for the first principal component stored in the red channel, the second principal component in the green channel and the third principal component stored in the blue channel.

Fluorescence Image Processing

A consistent area of interest was defined for each zoom level to exclude the pot and non-uniform areas of the imaging chamber backdrop. Within that area, pixels with an intensity value greater than 70 in the red channel were considered to be plant pixels. The aggregate fluorescence intensity was defined as the sum of the red channel intensity values for all pixels classified as plant pixels within the region of interest, and the mean fluorescence intensity as the aggregate fluorescence intensity value divided by the number of plant pixels within the region of interest.

Plant Biomass Prediction

Two methods were used to predict plant biomass. The first was a single variable model based on the number of zoom level adjusted plant pixels identified in the two RGB side view images on a given day. The second was a multivariate model based upon the sum of plant pixels identified in the two RGB side views, sum of plant pixels identified in the two RGB side views plus the RGB top view, aggregate fluorescence intensity in the two side views, aggregate fluorescence intensity in the two side views plus the top view, number of plant stem pixels identified in the hyperspectral image and number of plant leaf pixels identified in the hyperspectral image. Traits were selected to overlap with those employed by [14] where possible. This multivariate dataset was used to predict plant biomass using linear modeling as well as MARS, Random Forest and SVM [14]. MARS analysis was performed using the R package earth [15], Random Forest with the R package randomForest [16] and SVM with the R package e1071 [17].

Data Validation and Quality Control

Validation against ground truth measurements

A total of approximately 500 GB of image data was initially generated by the system during the course of this experiment consisting of RGB images (51.1%), fluorescence images (4.3%), and hyperspectral images (44.6%). A subset of the RGB images within this dataset were previously analyzed in [18], and were made available for download from <http://plantvision.unl.edu/dataset> under the terms of the Toronto Agreement. To validate the dataset and ensure plants had been properly tracked through both the automated imaging system and ground truth measurements, a simple script was written to segment images into plant and not-plant pixels (Figure 1). Source codes for all validation analysis are posted online (https://github.com/shanwai1234/Maize_Phenotype_Map).

Based on the segmentation of the image into plant and non-plant pixels, plant height was scored as the y axis dimension of the minimum bounding box. Plant area was scored as the total

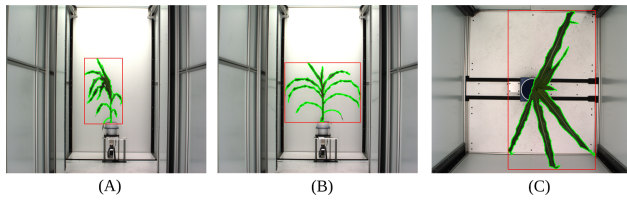


Figure 1. Segmentation of images into plant and not plant pixels for one representative plant (Path to this image in the released dataset: Genotype_ZL019 -> Plant_008-19 -> Image_Type -> Day_32). The area enclosed by green border is composed of pixels scored as "plant", the area outside the green border is composed of pixels scored as "not-plant". Minimum bounding rectangle of plant pixels is shown in red. (A) Side view, angle 1; (B) Side view, 90 degree rotation relative to A; (C) Top View.

number of plant pixels observed in both side view images after correcting for the area of each pixel at each zoom employed (See Methods). Similar approaches to estimate plant biomass have been widely employed across a range of grain crop species including rice [19], wheat [20], barley [20, 21], maize [12], sorghum [22] and setaria [9]. Calculated values were compared to manual measurements of plant height and plant fresh biomass which were quantified using destructive methods on the last day of the experiment. In both cases manual measurements and image derived estimates were highly correlated, although the correlation between manual and estimated height was greater than the correlation between manually measured and estimated biomass (Figure 2A,B). Using the PlantCV software package [23], equivalent correlations between estimated and ground truth biomass were obtained ($r=0.91$). Estimates of biomass using both software packages were more correlated with each other ($r=0.96$) than either was with ground truth measurements. This suggests that a significant fraction of the remaining error is the result of the expected imperfect correlation between plant size and plant mass, rather than inaccuracies in estimating plant size using individual software packages. Recent reports have suggested that estimates of biomass incorporating multiple traits extracted from image data can increase accuracy [14]. We tested the accuracy of biomass prediction of four multivariate estimation techniques on this dataset (see Methods). The correlation coefficient (r value) of the estimated biomass measures with ground truth data was 0.949, 0.958, 0.925 and 0.951 for multivariate linear model, MARS, Random Forest and SVM respectively.

The residual value – difference between the destructively measured biomass value and the predicted biomass value based on image data and the linear regression line equation – was calculated for each individual plant (Figure 2C). Using data from the multiple replicates of each individual accession, the proportion of error which is controlled by genetic factors rather than random error can be ascertained. We determined that 58% of the total error in biomass estimate was controlled by genetic variation between different maize lines. As such, this error is systematic rather than random and thus more likely to produce misleading downstream results when used in quantitative genetic analysis. As mentioned above, biomass and plant size are imperfectly correlated, as different plants can exhibit different densities, for example as a result of different leaf to stem ratios. Recent reports have suggested that estimates of biomass incorporating multiple traits extracted from image data can increase accuracy [14]. We tested the accuracy of biomass prediction of four multivariate estimation techniques on this dataset (see Methods). The correlation of the estimated biomass measures with ground truth data was 0.949, 0.958, 0.925 and 0.951 for multivariate linear model, MARS, Random Forest and SVM respectively. However, even when employing the most accurate of these four methods (MARS), 63% of the error in biomass es-

timation could be explained by genetic factors. This source of error, with the biomass of some lines systematically underestimated and the biomass of other lines systematically overestimated presents a significant challenge to downstream quantitative genetic analysis. Given the prevalence of plant pixel counts as a proxy for biomass [20, 22, 9, 21, 12, 19].

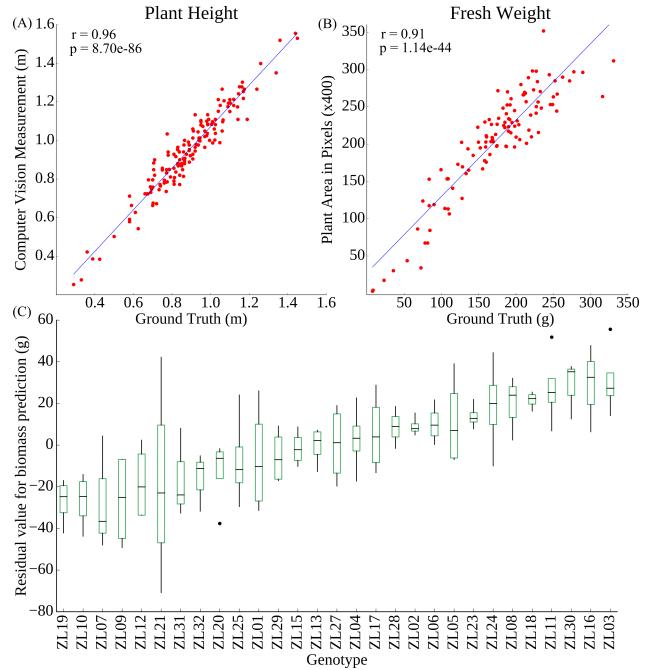


Figure 2. Correlation between image-based and manual measurements of individual plants. (A) Plant height; (B) Plant fresh biomass; (C) Variation in the residual between estimated biomass and ground truth measurement of biomass across inbreds.

Patterns of change over time

One of the desirable aspects of image based plant phenotyping is that, unlike destructively measured phenotypes, the same plant can be imaged repeatedly. Instead of providing a snapshot in time this allows researchers to quantify rates of change in phenotypic values over time, providing an additional set of derived trait values. Given the issues with biomass quantification presented above, measurements of plant height were selected to validate patterns of change in phenotypic values over time. As expected, height increases over time, and the patterns of increase tended to cluster together by genotype (Figure 3A). Increases in height followed by declines, as observed for ZL26, were determined to be caused by a change in the angle of the main stalk. While the accuracy of height estimates was assessed by comparison to physical ground truth measurements only on the last day, the height of three randomly selected plants (Plant 007-26, Plant 002-7 and Plant 041-29) were manually measured from image data and compared to software based height estimates, and no significant differences were observed between the manual and automated measurements (Figure 3B; Supplementary Table 1). To perform a similar test of the accuracy of biomass estimation at different stages in the maize life cycle, a set of existing ground truth measurements for two genotypes under two stress treatments [12] were combined with additional later grow stage data (Supplemental Table 2). The correlation between total plant pixels observed in the two side views and plant biomass was actually substantially higher in this dataset ($r=0.97$) than the primary dataset, likely as a result of the smaller amount of genetic vari-

ability among these plants (Supplementary Figure 1).

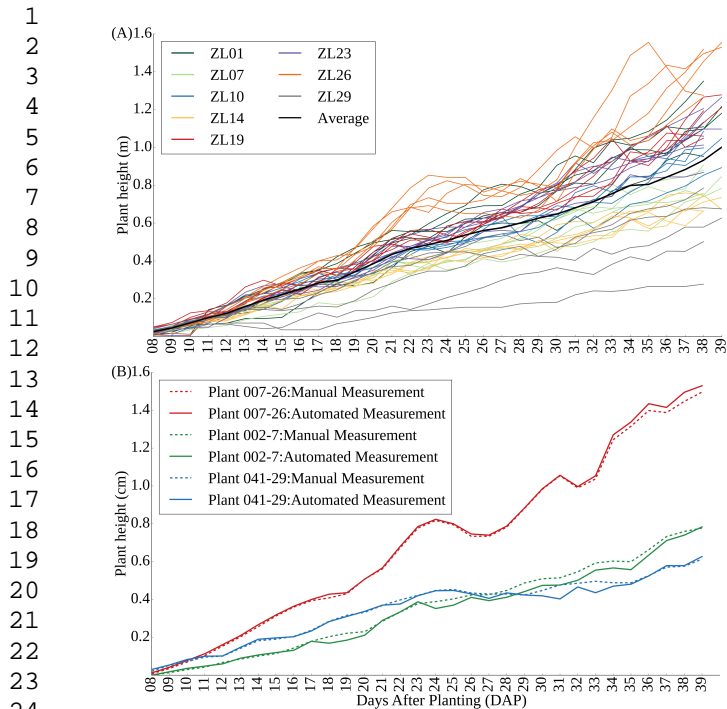


Figure 3. (A) Plant growth curves of each of five replicates of eight selected genotypes; (B) Comparison of manual measurements of plant height from image data with automated measurements for three randomly selected plants on each day of the experiment.

Heritability of phenotypes

The proportion of total phenotypic variation for a trait controlled by genetic variation is referred to as the heritability of that trait and is a good indicator of how easy or difficult it will be to either identify the genes which control variation in a given trait, or to breed new crop varieties in which a given trait is significantly altered. Broad-sense heritability can be estimated without the need to first link specific genes to variation in specific traits [24]. Variation in a trait which is not controlled by genotype can result from environmental effects, interactions between genotype and environment, random variance, and measurement error. Controlling for estimated row effects on different phenotypic measurements significantly increased overall broad sense heritability (Figure 4A,B). This result suggests that even within controlled environments such as greenhouses, significant micro-environmental variation exists and that proper statistically based experimental design remains critical importance in even controlled environment phenotyping efforts.

If the absolute size of measurement error was constant in this experiment, as the measured values for a given trait became larger, the total proportion of variation explained by the error term should decrease and, as a result, heritability should increase as observed (Figure 4A). This trend was indeed observed across six different phenotypic measurements (three traits calculated from each of two viewing angles (Figure 4B). Plant height also exhibited significantly greater heritability when calculated solely from the 90 degree side angle photo than when calculated solely from to 0 degree angle photo.

In previous studies, fluorescence intensity has been treated as an indicator for plant abiotic stress status [25, 26, 7, 27] or chlorophyll content level [28, 29]. Using the fluorescence

images collected as part of this experiment, the mean fluorescence intensity value for each plant image was calculated (see Methods). We found that this trait exhibited moderate heritability, with the proportion of variation controlled by genetic factors increasing over time and reaching approximately 60% by the last day of the experiment (Figure 4B).

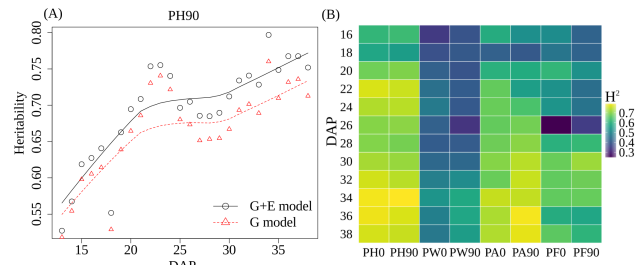


Figure 4. (A) The time course broad sense heritability of PH90. The heritability in the G model was calculated using a linear model that only considers the effect of genotype with residual values in the error term while heritability in the G + E model was calculated using a linear model that considers the effect of both genotype and environment (row effect) with residual values in the error term.; (B) The time course broad sense heritability (H^2) after controlling row effects for 6 trait measurements every second day across the phenotyping cycle. PA0: Plant Area in 0 degree (The major axis of leaf phylotaxy was parallel to the camera at 0 degree); PA90: Plant Area in 90 degree (The major axis of leaf phylotaxy was perpendicular to the camera at 90 degree); PH0: Plant Height in 0 degree; PH90: Plant Height in 90 degree; PW0: Plant Width in 0 degree; PW90: Plant Width in 90 degree; PF0: Average of plant fluorescence intensity in 0 degree; PF90: Average of plant fluorescence intensity in 90 degree.

Hyperspectral image validation

Hyperspectral imaging of crop plants has been employed previously in field settings using airborne cameras [30, 31, 32]. As a result of the architecture of grain crops such as maize, aerial imagery will largely capture leaf tissue during vegetative growth, and either tassels (maize) or seed heads (sorghum, millet, rice, oats, etc) during reproductive growth. The dataset described here includes hyperspectral imagery taken from the side of individual plants, enabling quantification of the reflectance properties of plant stems in addition to leaf tissue.

Many uses of hyperspectral data reduce the data from a whole plant or whole plot of genetically identical plants to a single aggregate measurement. While these approaches can increase the precision of intensity measurements for individual wavelengths, these approaches also sacrifice spatial resolution and can in some cases produce apparent changes in reflectivity between plants that result from variation in the ratios of the sizes of different organs with different reflective properties. To assess the extent of variation in the reflectance properties of individual plants, a principal component analysis of variation in intensity values for individual pixels was conducted. After non-plant pixels were removed from the hyperspectral data cube (Figure 5A) (See Methods), false color images were generated encoding the intensity values of the first three principal components of variation as the intensity of the red, green, and blue channels respectively (Figure 5B, C and D). The second principal component (green channel) marked boundary pixels where intensity values likely represent a mixture of reflectance data from the plant and from the background. The first principal component (red channel) appeared to indicate distinctions between pixels within the stem of the plant and pixels within the leaves.

Based on this observation, an index was defined which accurately separated plant pixels into leaf and stem (see Methods).

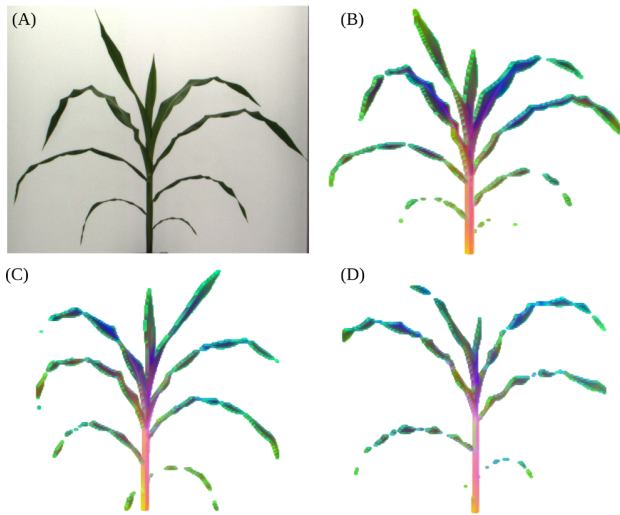


Figure 5. Segmentation and visualization of variation in hyperspectral signatures of representative maize plant images. (A) RGB photo of Plant 013-2 (ZL02) collected on DAP 37; (B) False color image constructed of the same corn plant from a hyperspectral photo taken on the same day. For each plant pixel the values for each of the first three principal components of variation across 243 specific wavelength intensity values are encoded as one of the three color channels in the false image; (C) Equivalent visualization for Plant 048-9 (ZL09); (D) Equivalent visualization for Plant 008-19 (ZL19).

Stem pixels were segmented from the rest of the plant using an index value derived from the difference in intensity values observed in the 1056nm and 1151nm hyperspectral bands. This methodology was previously described [12]. The reflectance pattern of individual plant stems is quite dissimilar from the data observed from leaves and exhibits significantly different reflective properties in some areas of the near infrared (Figure 6). Characteristics of the stem are important breeding targets for both agronomic traits (lodging resistance, yield for biomass crops) and value added traits (biofuel conversion potential for bioenergy crops, yield for sugarcane and sweet sorghum). Hyperspectral imaging of the stem has the potential to provide nondestructive measurements of these traits. The calculated pattern of leaf reflectance for the data presented here are comparable with those observed in field-based hyperspectral studies [33, 34, 35], providing both external validation and suggesting that the data presented here may be of use in developing new indices for use under field conditions.

In conclusion, while the results presented above highlight some of the simplest traits which can be extracted from plant image data, these represent a small fraction of the total set of phenotypes for which image analysis algorithms currently exist, and those in turn represent a small fraction of the total set of phenotypes which can potentially be scored from image data. Software packages already exist to measure a range of plant architectural traits such as leaf length, angle, and curvature from RGB images [6, 36]. Tools are also being developed to extract phenotypic information on abiotic stress response patterns from fluorescence imaging [6, 7]. The analysis of plant traits from hyperspectral image data, while common place in the remote sensing realm where an entire field may represent a single data point, is just beginning for single plant imaging. Recent work as highlighted the potential of hyperspectral imaging to quantify changes in plant composition and nutrient content throughout development [12, 37]. While these techniques have great potential to accelerate efforts to link genotype to phenotype through ameliorating the current bottleneck of plant phenotypic data collection, it will be important to balance the development of new image analysis tools with the awareness of the potential for systematic error result-

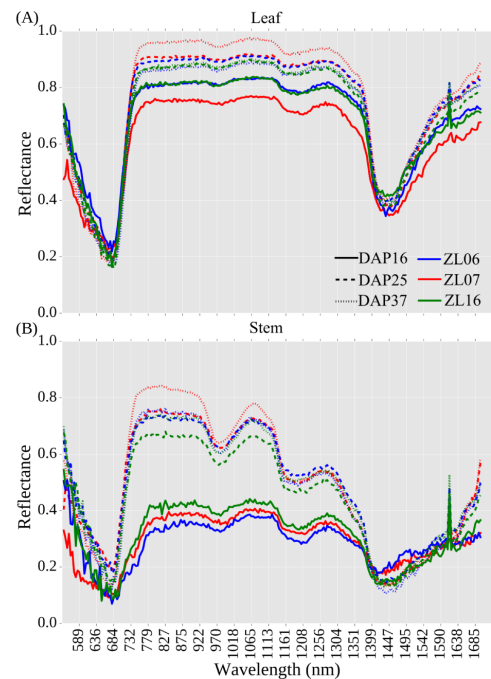


Figure 6. Reflectance values for three plants - Plant 090-6 (ZL06), Plant 002-7 (ZL07), and Plant 145-16 (ZL16) on three days across development. (A) Reflectance values for non-stem plant pixels (i.e. leaves) (B) Reflectance values for pixels within the plant stem.

ing from genetic variation between different lines of the same crop species.

Availability of source code and requirements

- Project name: Maize Phenotype Map
- Project home page: https://github.com/shanwai1234/Maize_Phenotype_Map
- Operating system(s): Linux
- Programming language: Python 2.7
- Other requirements: OpenCV module 2.4.8, Numpy >1.5, CMake > 2.6, GCC > 4.4.x, Scipy 0.13
- License: BSD 3-Clause License

Availability of supporting data and materials

The image data sets from four types of cameras, pot weight records per day and ground truth measurements with corresponding documentation for 32 maize inbreds and same types of image data for two maize inbreds under two stress treatments were deposited in the CyVerse data commons under a CC0 license with [38]. All image data were stored in the following data structure: Genotype -> Plant -> Camera type -> Day. For the hyperspectral camera each photo is stored as 243 sub images, each image representing intensity values for a given wavelength, so these require one additional level of nesting in the data structure Day -> wavelength. The grayscale images from the IR camera and the hyperspectral imaging system are stored as three-channel images with all three channels in a given pixel set to identical values. The fluorescence images contain almost all information in the red channel with the blue and green channel having intensities equal to or very close to zero, but data all three channels exist. Genotype data of 32 inbreds were generated as part of a separate project and SNP calls for individual inbred lines were made available either through

[39] or the ZeaGBSv2.7 GBS SNP dataset stored in Panzea. Measurements for thirteen core phenotypes at each field trial as well as local weather data can be retrieved from publicly released Genomes 2 Fields datasets released on CyVerse [39, 40]. Data from the 2014 G2F field trials is posted [39] and data from the 2015 G2F field trials is posted [40]. Genetically identical seeds from the majority of the accessions used in creating both this dataset and the Genomes 2 Fields field trial data can be ordered from public domain sources (e.g. USDA GRIN) and are listed in Table 1. Further supporting metadata and snapshots of the Maize Phenotype Map code are available in the GigaScience database, GigaDB [41].

Declarations

List of abbreviations

DAP: Days after planting
 GBS: Genotyping by Sequencing
 LED: Light-emitting diode
 MARS: Multivariate Adaptive Regression Splines
 NDVI: Normalized difference vegetation index
 NIR: Near-infrared
 RGB: An image with separate intensity values for the red, blue and green channels
 SNP: Single Nucleotide Polymorphism
 SVM: Support Vector Machines
 UNL: University of Nebraska-Lincoln
 PA0: Plant Area calculated from a 0 degree image. Plants were initially orientated then leaves would be arranged parallel to the camera at 0 degrees.
 PA90: Plant Area calculated from a 90 degree image. Plants were initially orientated then leaves would be arranged perpendicular to the camera at 90 degrees.
 PCA: Principal Component Analysis
 PH0: Plant Height calculated from a 0 degree image
 PH90: Plant Height calculated from a 90 degree image
 PW0: Plant Width calculated from a 0 degree image
 PW90: Plant Width calculated from a 90 degree image
 PFO: Average of plant fluorescence intensity in 0 degree
 PF90: Average of plant fluorescence intensity in 90 degree.

Consent for publication

Not applicable.

Competing Interests

The authors declare that they have no competing interests.

Funding

This research was supported by the Nebraska Corn Board (Award #88-R-1617-03), the Iowa Corn Board (Award #), the National Science Foundation under Grant No. OIA-1557417, and Internal University of Nebraska funding to JCS. The sources of funding have no role in the design of the study and collection, analysis, and interpretation of data and in writing the manuscript.

Author's Contributions

JCS, and YQ designed the experiment; VS, JCS and ZL performed data acquisition; ZL, PP, YQ, YX, YG and JCS analyzed and interpreted the data; ZL and JCS produced and curated the metadata;

ZL and JCS implemented software; ZL and JCS prepared the initial draft. All authors reviewed the manuscript.

Acknowledgements

The authors are grateful to Yang Zhang, Xianjun Lai and Daniel WC Ngu for help in collecting manual measurements of plants, Thomas Hoban for manually counting pixels of selected plant images, Kent M. Eskridge for valuable discussions on experimental design, Addie Thompson, Jinliang Yang for assistance on heritability analysis, and the members of the Genomes 2 Fields consortium for sharing both seed and datasets prior to publication. CyVerse is supported by the U.S. National Science Foundation under award numbers DBI-0735191 and DBI-1265383.

References

- Grassini P, Eskridge KM, Cassman KG. Distinguishing between yield advances and yield plateaus in historical crop production trends. *Nature communications* 2013;4:2918.
- Hartmann A, Czauderna T, Hoffmann R, Stein N, Schreiber F. HTPheno: an image analysis pipeline for high-throughput plant phenotyping. *BMC bioinformatics* 2011;12(1):148.
- Topp CN, Iyer-Pascuzzi AS, Anderson JT, Lee CR, Zurek PR, Symonova O, et al. 3D phenotyping and quantitative trait locus mapping identify core regions of the rice genome controlling root architecture. *Proceedings of the National Academy of Sciences* 2013;110(18):E1695-E1704.
- Das A, Schneider H, Burrige J, Ascanio AKM, Wojciechowski T, Topp CN, et al. Digital imaging of root traits (DIRT): a high-throughput computing and collaboration platform for field-based root phenomics. *Plant methods* 2015;11(1):51.
- Zhang X, Huang C, Wu D, Qiao F, Li W, Duan L, et al. High-throughput phenotyping and QTL mapping reveals the genetic architecture of maize plant growth. *Plant physiology* 2017;p. pp-01516.
- Chen D, Neumann K, Friedel S, Kilian B, Chen M, Altmann T, et al. Dissecting the phenotypic components of crop plant growth and drought responses based on high-throughput image analysis. *The Plant Cell* 2014;26(12):4636-4655.
- Campbell MT, Knecht AC, Berger B, Brien CJ, Wang D, Walia H. Integrating image-based phenomics and association analysis to dissect the genetic architecture of temporal salinity responses in rice. *Plant physiology* 2015;168(4):1476-1489.
- Munns R, James RA, Sirault XR, Furbank RT, Jones HG. New phenotyping methods for screening wheat and barley for beneficial responses to water deficit. *Journal of Experimental Botany* 2010;61(13):3499-3507.
- Fahlgren N, Feldman M, Gehan MA, Wilson MS, Shyu C, Bryant DW, et al. A versatile phenotyping system and analytics platform reveals diverse temporal responses to water availability in *Setaria*. *Molecular plant* 2015;8(10):1520-1535.
- Lobet G, Draye X, Périlleux C. An online database for plant image analysis software tools. *Plant methods* 2013;9(1):38.
- Campbell D, de Leon N, Edwards J, Gardiner J, Al Khalifah N, Lawrence-Dill C, et al. Genomes to Fields 2016 data release. *CyVerse Data Commons* 2016;.
- Ge Y, Bai G, Stoerger V, Schnable JC. Temporal dynamics of maize plant growth, water use, and leaf water content using automated high throughput RGB and hyperspec-

- tral imaging. *Computers and Electronics in Agriculture* 2016;127:625–632.
13. Gamon J, Surfus J. Assessing leaf pigment content and activity with a reflectometer. *New Phytologist* 1999;143(1):105–117.
 14. Chen D, Shi R, Pape JM, Klukas C. Predicting plant biomass accumulation from image-derived parameters. *bioRxiv* 2016;p. 046656.
 15. Milborrow S. *Earth: multivariate adaptive regression spline models*. R package version 2014;3:2–7.
 16. Liaw A, Wiener M, et al. Classification and regression by randomForest. *R news* 2002;2(3):18–22.
 17. Dimitriadou E, Hornik K, Leisch F, Meyer D, Weingessel A. *Misc Functions of the Department of Statistics (e1071)*, TU Wien. R package version 2005;p. 1–5.
 18. Choudhury SD, Stoerger V, Samal A, Schnable JC, Liang Z, Yu JG. Automated Vegetative Stage Phenotyping Analysis of Maize Plants using Visible Light Images. *Data Science for Food, Energy and Water workshop*, San Francisco, California, USA, August 2016;.
 19. Al-Tamimi N, Brien C, Oakey H, Berger B, Saade S, Ho YS, et al. Salinity tolerance loci revealed in rice using high-throughput non-invasive phenotyping. *Nature communications* 2016;7.
 20. Golzarian MR, Frick RA, Rajendran K, Berger B, Roy S, Tester M, et al. Accurate inference of shoot biomass from high-throughput images of cereal plants. *Plant methods* 2011;7(1):2.
 21. Honsdorf N, March TJ, Berger B, Tester M, Pillen K. High-throughput phenotyping to detect drought tolerance QTL in wild barley introgression lines. *PLoS one* 2014;9(5):e97047.
 22. Neilson EH, Edwards A, Blomstedt C, Berger B, Møller BL, Gleadow R. Utilization of a high-throughput shoot imaging system to examine the dynamic phenotypic responses of a C₄ cereal crop plant to nitrogen and water deficiency over time. *Journal of experimental botany* 2015;66(7):1817–1832.
 23. Gehan MA, Fahlgren N, Abbasi A, Berry JC, Callen ST, Chavez L, et al. *PlantCV v2. 0: Image analysis software for high-throughput plant phenotyping*. PeerJ Preprints; 2017.
 24. Holland JB, Nyquist WE, Cervantes-Martínez CT. Estimating and interpreting heritability for plant breeding: an update. *Plant breeding reviews* 2003;22:9–112.
 25. Van Kooten O, Snel JF. The use of chlorophyll fluorescence nomenclature in plant stress physiology. *Photosynthesis research* 1990;25(3):147–150.
 26. Fracheboud Y, Haldimann P, Leipner J, Stamp P. Chlorophyll fluorescence as a selection tool for cold tolerance of photosynthesis in maize (*Zea mays* L.). *Journal of experimental botany* 1999;50(338):1533–1540.
 27. Kalaji HM, Jajoo A, Oukarroum A, Brestic M, Zivcak M, Samborska IA, et al. Chlorophyll a fluorescence as a tool to monitor physiological status of plants under abiotic stress conditions. *Acta Physiologiae Plantarum* 2016;38(4):102.
 28. Murchie EH, Lawson T. Chlorophyll fluorescence analysis: a guide to good practice and understanding some new applications. *Journal of experimental botany* 2013;64(13):3983–3998.
 29. Guanter L, Zhang Y, Jung M, Joiner J, Voigt M, Berry JA, et al. Global and time-resolved monitoring of crop photosynthesis with chlorophyll fluorescence. *Proceedings of the National Academy of Sciences* 2014;111(14):E1327–E1333.
 30. Zarco-Tejada P, Catalina A, González M, Martín P. Relationships between net photosynthesis and steady-state chlorophyll fluorescence retrieved from airborne hyperspectral imagery. *Remote Sensing of Environment* 2013;136:247–258.
 31. Zaman-Allah M, Vergara O, Araus J, Tarekegne A, Magorokosho C, Zarco-Tejada P, et al. Unmanned aerial platform-based multi-spectral imaging for field phenotyping of maize. *Plant methods* 2015;11(1):35.
 32. Yendrek C, Tomaz T, Montes CM, Cao Y, Morse AM, Brown PJ, et al. High-throughput phenotyping of maize leaf physiology and biochemistry using hyperspectral reflectance. *Plant physiology* 2016;p. pp–01447.
 33. Smith K, Steven M, Colls J. Use of hyperspectral derivative ratios in the red-edge region to identify plant stress responses to gas leaks. *Remote sensing of environment* 2004;92(2):207–217.
 34. Zhao D, Reddy KR, Kakani VG, Reddy V. Nitrogen deficiency effects on plant growth, leaf photosynthesis, and hyperspectral reflectance properties of sorghum. *European Journal of Agronomy* 2005;22(4):391–403.
 35. Baranowski P, Jedryczka M, Mazurek W, Babula-Skowronska D, Siedliska A, Kaczmarek J. Hyperspectral and thermal imaging of oilseed rape (*Brassica napus*) response to fungal species of the genus *Alternaria*. *PLoS one* 2015;10(3):e0122913.
 36. Klukas C, Chen D, Pape JM. Integrated analysis platform: an open-source information system for high-throughput plant phenotyping. *Plant physiology* 2014;165(2):506–518.
 37. Pandey P, Ge Y, Stoerger V, Schnable JC. High throughput in vivo analysis of plant leaf chemical properties using hyperspectral imaging. *Frontiers in Plant Science* 2017;8.
 38. Maize Image Phenotype Dataset Released in Association with this Paper; <https://doi.org/10.7946/P22K7V>.
 39. Publicly Released Genomes 2 Fields 2014 Field Trial Dataset; <https://doi.org/10.7946/P2V888>.
 40. Publicly Released Genomes 2 Fields 2015 Field Trial Dataset; <https://doi.org/10.7946/P24S31>.
 41. Liang Z, Pandey P, Stoerger V, Xu Y, Qiu Y, Ge Y, et al. Supporting data for "Conventional and hyperspectral time-series imaging of maize lines widely used in field trials". *GigaScience Database* 2017;<http://dx.doi.org/10.5524/100371>.

Supplementary Information

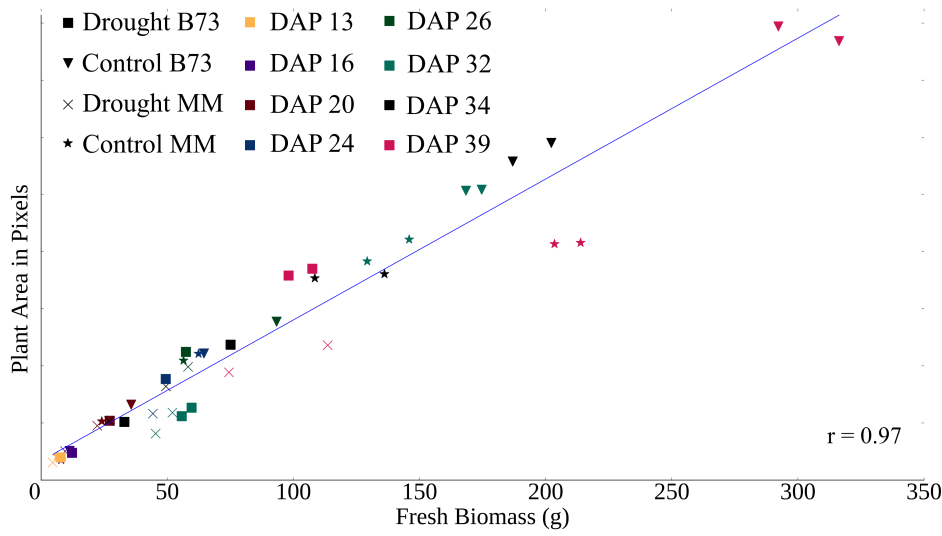


Figure S1. Correlation of fresh weight biomass with total number of plant pixels identified in two side view images for maize plants destructively sampled at eight different time points between 13 days and 39 days after planting (DAP).

1 1 **Conventional and hyperspectral time-series imaging of maize lines widely** 2 2 **used in field trials**

3
4
5
6
7
8 4 Zhikai Liang¹, Piyush Pandey², Vincent Stoerger³, Yuhang Xu⁴, Yumou Qiu⁴, Yufeng Ge² and
9 5 James C. Schnable^{1*}

10 6 1. Center for Plant Science Innovation, Department of Agronomy and Horticulture, University of
11 7 Nebraska-Lincoln, Lincoln, 68503, USA

12 8 2. Department of Biological System Engineering, University of Nebraska-Lincoln, Lincoln,
13 9 68503, USA

14 10 3. Plant Phenotyping Facilities Manager, University of Nebraska-Lincoln, Lincoln, 68503, USA

15 11 4. Department of Statistics, University of Nebraska-Lincoln, Lincoln, 68503, USA

16 12 *schnable@unl.edu

17 13 18 14 **Abstract**

19 15
20 16 **Background:** Maize (*Zea mays* ssp. *mays*) is one of three crops, along with rice and wheat,
21 17 responsible for more than 1/2 of all calories consumed around the world. Increasing the yield and
22 18 stress tolerance of these crops is essential to meet the growing need for food. The cost and speed
23 19 of plant phenotyping is currently the largest constraint on plant breeding efforts. Datasets linking
24 20 new types of high throughput phenotyping data collected from plants to the performance of the
25 21 same genotypes under agronomic conditions across a wide range of environments are essential
26 22 for developing new statistical approaches and computer vision based tools.

27 23
28 24 **Findings:** A set of maize inbreds – primarily recently off patent lines -- were phenotyped using a
29 25 high throughput platform at University of Nebraska-Lincoln. These lines have been previously
30 26 subjected to high density genotyping, and scored for a core set of 13 phenotypes in field trials
31 27 across 13 North American states in two years by the Genomes 2 Fields consortium. A total of
32 28 485 GB of image data including RGB, hyperspectral, fluorescence and thermal infrared photos
33 29 has been released.

34 30
35 31 **Conclusions:** Correlations between image-based measurements and manual measurements
36 32 demonstrated the feasibility of quantifying variation in plant architecture using image data.
37 33 However, naive approaches to measuring traits such as biomass can introduce nonrandom
38 34 measurement errors confounded with genotype variation. Analysis of hyperspectral image data
39 35 demonstrated unique signatures from stem tissue. Integrating heritable phenotypes from high-
40 36 throughput phenotyping data with field data from different environments can reveal previously
41 37 unknown factors influencing yield plasticity.

42 38 43 39 **Data Description**

44 40 **Background**

45 41
46 42 The green revolution created a significant increase in the yields of several major crops in the
47 43 1960s and 1970s, dramatically reducing the prevalence of hunger and famine around the world,
48
49
50
51
52
53
54
55
56
57
58
59
60
61
62
63
64
65

1
2
3
4 44 even as population growth continued. One of the major components of the green revolution was
5 45 new varieties of major grain crops produced through conventional phenotypic selection with
6 46 higher yield potentially. Since the green revolution, the need for food has continued to increase,
7 47 and a great deal of effort in the public and private sectors is devoted to developing crop varieties
8 48 with higher yield potential. However, as the low hanging fruit for increased yield vanish, each
9 49 new increase in yield requires more time and resources. Recent studies have demonstrated that
10 50 yield increases may have slowed or stopped for some major grain crops in large regions of the
11 51 world ^[1]. New approaches to plant breeding must be developed if crop production continues to
12 52 grow to meet the needs of an increasing population around the world.
13 53

14 54 The major bottleneck in modern plant breeding is phenotyping. Phenotyping can be used in two
15 55 ways. Firstly, by phenotyping a large set of lines, a plant breeder can identify those lines with the
16 56 highest yield potential and/or greatest stress tolerance in a given environment. Secondly,
17 57 sufficiently detailed phenotyping measurements from enough different plants can be combined
18 58 with genotypic data to identify regions of the genome of a particular plant species which carry
19 59 beneficial or deleterious alleles. The breeder can then develop new crop varieties which
20 60 incorporate as many beneficial alleles and exclude as many deleterious alleles as possible.
21 61 Phenotyping tends to be expensive and low throughput, yet as breeders seek to identify larger
22 62 numbers of alleles each with individually smaller effects, the amount of phenotyping required to
23 63 achieve a given increase in yield potential is growing. High throughput computer vision based
24 64 approaches to plant phenotyping have the potential to ameliorate this bottleneck. These tools can
25 65 be used to precisely quantify even subtle traits in plants and will tend to decrease in unit cost
26 66 with scale, while conventional phenotyping, which remains a human labor intensive processes,
27 67 does not.
28 68

29 69 Several recent pilot studies have applied a range of image-processing techniques to extract
30 70 phenotypic measurements from crop plants. RGB (R: Red channel; G: Green channel; B: Blue
31 71 channel) camera technology, widely used in the consumer sector, has also been the most widely
32 72 used tool in these initial efforts at computer vision based plant phenotyping ^[2,3,4,5]. Other types of
33 73 cameras including fluorescence ^[6,7] and NIR (near-infrared) ^[6,8,9] have also been employed in high
34 74 throughput plant phenotyping efforts, primarily in studies of the response of plant to different
35 75 abiotic stresses.
36 76

37 77 However, the utility of current studies is limited in two ways. Firstly, current analysis tools can
38 78 extract only a small number of different phenotypic measurements from images of crop plants.
39 79 Approximately 150 tools for analyzing plant image data are listed in a field specific database,
40 80 however the majority of these are either developed specifically for *Arabidopsis thaliana* which is
41 81 a model plant, or are designed specifically to analyze images of roots ^[10]. Secondly, a great deal
42 82 of image data is generated in controlled environments, however, there are comparatively few
43 83 attempts to link phenotypic measurements in the greenhouse to performance in the field.
44 84 However, one recent report in maize suggested that more than 50% of the total variation in yield
45 85 under field conditions could be predicted using traits measured under controlled environments
46 86 ^[10].
47 87

48 88 Advances in computational tools for extracting phenotypic measurements of plants from image
49 89 data and statistical models for predicting yield under different field conditions from such
50
51
52
53
54
55
56
57
58
59
60
61
62
63
64
65

1
2
3
4 90 measurements requires suitable training datasets. Here, we generate and validate such a dataset
5 91 consisting of high throughput phenotyping data from 32 distinct maize (*Zea mays*) accessions
6 92 drawn primarily from recently off-patent lines developed by major plant breeding companies.
7 93 These accessions were selected specifically because paired data from the same lines exists for a
8 94 wide range of plant phenotypes collected in 54 distinct field trials at locations spanning 13 North
9 95 American states or provinces over two years ^[11]. This extremely broad set of field sites captures
10 96 much of the environmental variation among areas in which maize are cultivated with total
11 97 rainfall during the growing season ranging from 133.604 mm to 960.628 mm (excluding sites
12 98 with supplemental irrigation) and peak temperatures during the growing season ranging from
13 99 23.5 °C to 34.9 °C. In addition, the same lines have been genotyped for approximately 200,000
14 100 SNP markers using GBS ^[11]. Towards these existing data, we added RGB, thermal infra-red,
15 101 fluorescent and hyperspectral images collected once per day per plant, as well as detailed water-
16 102 use information (single day, single plant resolution). At the end of the experiment, 12 different
17 103 types of ground-truth phenotypes were measured for individual plants including destructive
18 104 measurements. A second experiment focused on interactions between genotype and
19 105 environmental stress, collecting the same types of data described above from two maize
20 106 genotypes under well watered and water stressed conditions ^[12]. We are releasing this curated
21 107 dataset of high throughput plant phenotyping images from accessions where data on both
22 108 genotypic variation and agronomic performance under field conditions is already available. All
23 109 data was generated using a Lemnatec designed high throughput greenhouse-based phenotyping
24 110 system constructed at the University of Nebraska-Lincoln. This system is distinguished from
25 111 existing public sector phenotyping systems in North America by both the ability to grow plants
26 112 to a height of 2.5 meters and the incorporation of a hyperspectral camera ^[9]. Given the unique
27 113 properties described above, this comprehensive data set should lower the barriers to the
28 114 development of new computer vision approaches or statistical methodologies by independent
29 115 researchers who do not have the funding or infrastructure to generate the wide range of different
30 116 types of data needed.
31
32
33
34
35
36
37
38

39 118 **Methods**

40 119 41 42 120 **Greenhouse Management**

43 121
44 122 All imaged plants were grown in the greenhouse facility of the University of Nebraska-Lincoln's
45 123 Greenhouse Innovation Center (Latitude: 40.83, Longitude: -96.69) between October 2nd, 2015
46 124 to November 10th, 2015. Kernels were sown in 1.5 gallon pots with Fafard germination mix
47 125 supplemented with 1 cup (236 mL) of Osmocote plus 15-9-12 and one tablespoon (15 mL) of
48 126 Micromax Micronutrients per 2.8 cubic feet (80 L) of soil. The target photoperiod was 14:10
49 127 with supplementary light provided by LED growth lamps from 07:00 to 21:00 each day. The
50 128 target temperature of the growth facility was between 24-26 °C. Pots were weighed once per day
51 129 and watered back to a target weight of 5,400 grams from 10-09-2015 to 11-07-2015 and a target
52 130 weight of 5,500 grams from 11-08-2015 to the termination of the experiment.
53
54
55
56
57

58 132 **Experimental Design**

59 133
60
61
62
63
64
65

A total of 156 plants, representing the 32 genotypes listed in Table 1 were grown and imaged, as well as 4 pots with soil but no plant which serve as controls for the amount of water lost from soil as a result of non-transpiration mechanisms (e.g. evaporation). The 156 plants plus control pots were arranged in a ten row by sixteen column grid, with 0.235 meter spacing between plants in the same row and 1.5 meters spacing between rows (Table 2). Sequential pairs of two rows were consisted of a complete replicate with either 31 genotypes and one empty control pot, or 32 genotypes. Within each pair of rows, genotypes were blocked in groups of eight (one half row), with order randomized within blocks between replicates in order to maximize statistical power to analyze within-greenhouse variation.

Table 1. 32 genotypes in maize phenotype map

| Genotype ID | Genotype | Source | Released Year |
|-------------|----------|---------------------|---------------|
| ZL1 | 740 | Novartis Seeds | 1998 |
| ZL2 | 2369 | Cargill | 1989 |
| ZL3 | A619 | Public Sector | 1992 |
| ZL4 | A632 | Public Sector | 1992 |
| ZL5 | A634 | Public Sector | 1992 |
| ZL6 | B14 | Public Sector | 1968 |
| ZL7 | B37 | Public Sector | 1971 |
| ZL8 | B73 | Public Sector | 1972 |
| ZL9 | C103 | Public Sector | 1991 |
| ZL10 | CM105 | Public Sector | 1992 |
| ZL11 | LH123HT | Holden's Foundation | 1984 |
| ZL12 | LH145 | Holden's Foundation | 1983 |
| ZL13 | LH162 | Holden's Foundation | 1990 |
| ZL14 | LH195 | Holden's Foundation | 1989 |
| ZL15 | LH198 | Holden's Foundation | 1991 |
| ZL16 | LH74 | Holden's Foundation | 1983 |
| ZL17 | LH82 | Holden's Foundation | 1985 |
| ZL18 | Mo17 | Public Sector | 1964 |
| ZL19* | DKPB80 | DEKALB Genetics | ? |
| ZL20 | PH207 | Pioneer Hi-Bred | 1983 |
| ZL21 | PHB47 | Pioneer Hi-Bred | 1983 |
| ZL22** | PHG35 | Pioneer Hi-Bred | 1983 |
| ZL23 | PHG39 | Pioneer Hi-Bred | 1983 |
| ZL24 | PHG47 | Pioneer Hi-Bred | 1986 |
| ZL25 | PHG83 | Pioneer Hi-Bred | 1985 |
| ZL26 | PHJ40 | Pioneer Hi-Bred | 1986 |
| ZL27 | PHN82 | Pioneer Hi-Bred | 1989 |
| ZL28 | PHV63 | Pioneer Hi-Bred | 1988 |
| ZL29 | PHW52 | Pioneer Hi-Bred | 1988 |
| ZL30 | PHZ51 | Pioneer Hi-Bred | 1986 |
| ZL31 | W117HT | Public Sector | 1982 |
| ZL32 | Wf9 | Public Sector | 1991 |

* Not currently available for order

** Genotype represented by only a single plant in the dataset

Table 2. Experimental layout (ID: ZL1-ZL32). At the time this experiment was conducted, the total size of the UNL greenhouse system was ten rows by twenty columns. Positions marked with UP indicate pots filled with plants from an unrelated experiment, while positions marked with NA indicate pots which had no plants. The first complete replicate is shown in color, and the four incomplete blocks within the first replicate are marked in different colors. * marks empty pots within the experimental design.

| | | | | | | | | | | | | | | | | | | | |
|----|----|----|----|----|----|----|----|----|----|----|----|----|----|----|----|----|----|----|----|
| 9 | 7 | 3 | 10 | 23 | 25 | 26 | 19 | 13 | 5 | 29 | 21 | 2 | 4 | 18 | 20 | UP | UP | UP | UP |
| 11 | 16 | 1 | 32 | 17 | 27 | 6 | 22 | 24 | 31 | 14 | 30 | 15 | 28 | 8 | 12 | UP | UP | UP | UP |
| 29 | 31 | 15 | 13 | 1 | 17 | 25 | 9 | 21 | 30 | 3 | 5 | * | 19 | 14 | 6 | UP | UP | UP | UP |
| 12 | 23 | 32 | 16 | 7 | 28 | 2 | 18 | 10 | 11 | 8 | 26 | 27 | 4 | 20 | 24 | UP | UP | UP | UP |
| 25 | 9 | 21 | 27 | 28 | 12 | 5 | 11 | 15 | 6 | * | 7 | 4 | 23 | 31 | 20 | UP | UP | UP | UP |
| 19 | 32 | 29 | 24 | 16 | 13 | 3 | 8 | 17 | 14 | 18 | 30 | 10 | 26 | 1 | 2 | UP | UP | UP | UP |
| 8 | 1 | 17 | 23 | 21 | 5 | 7 | 24 | 27 | 18 | 3 | 11 | 31 | 15 | 19 | 2 | NA | NA | NA | NA |
| 25 | 30 | 4 | 9 | 16 | 32 | 14 | 20 | * | 10 | 6 | 29 | 28 | 12 | 26 | 13 | NA | NA | NA | NA |
| 15 | 10 | 5 | 32 | 31 | 21 | 16 | 26 | 2 | 18 | 9 | 25 | 6 | 8 | 24 | * | NA | NA | NA | NA |
| 29 | 13 | 23 | 14 | 27 | 7 | 11 | 30 | 12 | 1 | 28 | 4 | 3 | 20 | 17 | 19 | NA | NA | NA | NA |

Plant Imaging

The plants were imaged daily using four different cameras in separate imaging chambers. The four types of cameras were thermal infrared, fluorescence, conventional RGB, and hyperspectral [12]. Images were collected in the order that the camera types are listed in the previous sentence. On each day, plants were imaged sequentially by row, starting with row 1 column 1 and concluding with row 10, column 16 (Table 2).

Plants were imaged from the side at two angles offset 90 degrees from each other as well as a top down view. On the first day of imaging or when plants reached the two leaf stage of development, the pot was rotated so that the major axis of leaf phylotaxy was parallel to the camera in the PA0 orientation and perpendicular to the camera in the PA90 orientation. This orientation is consistent for all cameras and was not adjusted again for the remainder of the experiment. The fluorescence camera captured images with a resolution of 1038×1390 pixels and measures emission intensity at wavelengths between 500-750 nm based on excitation with light at 400-500 nm. Plants were imaged using the same three perspectives employed for the thermal infrared camera. The RGB camera captured images with a resolution of 2454×2056 pixels. Initially the zoom of the RGB camera in side views was set such that each pixel corresponds to 0.746 mm at the distance of the pot from the camera. Between 2015-11-05 and 2015-11-10, the zoom level of the RGB camera was reduced to keep the entire plant in the frame of the image. As a result of a system error, this same decreased zoom level was also applied to all RGB images taken on 2015-10-20. At this reduced zoom level, each pixel corresponds to 1.507 mm at the distance of the pot from the camera, an approximate 2x change. Plants were also imaged using the same three perspectives employed for the thermal infrared camera. The hyperspectral camera captured images with a resolution of 320 horizontal pixels. As a result of the scanning

1
2
3
4 182 technology employed, vertical resolution ranged from 494 to 499 pixels. Hyperspectral imaging
5 183 was conducted using illumination from halogen bulbs (Manufacturer Sylvania, model # ES50
6 184 HM UK 240V 35W 25°GU10). A total of 243 separate intensity values were captured for each
7 185 pixel spanning a range of light wavelengths between 546nm-1700nm. Data from each
8 186 wavelength was stored as a separate grayscale image.
9 187

10 187 11 188 **Ground Truth Measurement**

12 188
13 189
14 190 Ground truth measurements were collected at the termination of data collection on November
15 191 11-12, 2015. Manually collected phenotypes included plant height, total number of visible
16 191 leaves, number of total fully extended leaves, stem diameter at the base of the plant, stem
17 192 diameter at the collar of the top fully extended leaf, length and width of top fully extended leaf,
18 193 and presence/absence visible anthocyanin production in the stem. After these measurements,
19 194 total above-ground fresh weight biomass was measured for four out of five replicates, resulting
20 195 in the destruction of the plants. Ground truth data for the drought stressed subset of this dataset
21 196 was collected following the procedure previously described in ^[12].
22 196
23 197
24 197
25 198

26 199 **RGB Image Processing**

27 200
28 201 Pixels covering portions of the plant were segmented out of RGB images using a green index
29 202 $((2 \times G)/(R+B))$. Pixels with an index value greater than 1.15 ^[12] were considered to be plant
30 202 pixels. This method produced some false positive plant pixels within the reflective metal
31 203 columns at the edge of the image. To reduce the impact of false positives, these areas were
32 204 excluded from the analysis. Therefore, when plant leaves cross the reflective metal frame, some
33 205 true plant pixels were excluded. If no plant pixels were identified in the image - often the case in
34 206 the first several days when the plant had either not germinated or had not risen above the edge of
35 207 the pot - the value was recorded as "NA" in the output file.
36 207
37 208
38 209

39 210 **Heritability Analysis**

40 210
41 211
42 212 A linear regression model was used to analyze the genotype effect (excluding genotype ZL22
43 213 which lacked replication) and greenhouse position effect on plant traits. The responses were
44 214 modeled independently for each day as

$$45 214 \quad y_{h,ij,t} = \mu_{h,t} + \alpha_{h,i,t} + \gamma_{h,v(i,j),t} + \varepsilon_{h,ij,t} \quad (1)$$

46 215
47 216 where the subscript $h=1, \dots, 6$ denotes the three responses extracted from the images: plant height,
48 217 width and size for the two views 0 and 90 degree. The subscripts i, j and t denote the j th plant in
49 217 the i th row and day t , respectively, and $v(i,j)$ stands for the genotype at this pot. The parameters α
50 218 and γ denote row effect and genotype effect, respectively. The error term is $\varepsilon_{h,ij,t}$. Let $SS_{\alpha,t}$, $SS_{\gamma,t}$
51 219 and $SS_{\varepsilon,t}$ be the sum of squares of the regression model (1) for the row effect, genotype effect
52 220 and the error at time t , respectively. Let $SS_t = SS_{\alpha,t} + SS_{\gamma,t} + SS_{\varepsilon,t}$ be the total sum of squares at
53 221 time t . The heritability HR_t (2) of a given trait within this population was defined as the ratio of
54 222 the genotype sum of squares over the sum of genotype and error sum of squares. For the estimate
55 222 of the heritability of measurement error, the row effect term was replaced by a replicate effect
56 223 (each replicate consisted of two sequential rows) with exclusion of ZL22 as only one plant of this
57 224 genotype was grown.
58 224
59 225
60 226
61
62
63
64
65

1
2
3
4
5
6
7
8
9
10
11
12
13
14
15
16
17
18
19
20
21
22
23
24
25
26
27
28
29
30
31
32
33
34
35
36
37
38
39
40
41
42
43
44
45
46
47
48
49
50
51
52
53
54
55
56
57
58
59
60
61
62
63
64
65

227
228
229
230
231
232
233
234
235
236
237
238
239
240
241
242
243
244
245
246
247
248
249
250
251
252
253
254
255
256
257
258
259
260
261
262
263
264
265
266
267
268
269

$$HR_t = \frac{SS_{\gamma,t}}{SS_{\epsilon,t} + SS_{\gamma,t}} \quad (2)$$

As the heritability index may change over the growth of the plant, a nonparametric smoothing method was provided for analyzing the time varying heritability of plants. The definition in (3) excludes the variation brought by the greenhouse row effect, which can be considered as the percentage of the variation in plant response that can be explained by the genotype effect after adjusting the environmental effect. To compare with this definition of heritability (2) the response in the model without considering the row effect was constructed as

$$y_{h,ij,t} = \mu_{h,t} + \gamma_{h,v(i,j),t} + \epsilon_{h,ij,t} \quad (3)$$

where similarly as (1), $v(i,j)$ is the genotype of the j th plant in the i th row. Let $\widetilde{SS}_{\gamma,t}$ and \widetilde{SS}_t be the genotype sum of squares and total sum of squares under (4). The classical heritability is defined as $\widetilde{SS}_{\gamma,t}$

$$HR_t = \frac{\widetilde{SS}_{\gamma,t}}{\widetilde{SS}_t} \quad (4)$$

Hyperspectral Image Processing

Two methods and thresholds were used to extract plant regions of interest from hyperspectral images. First, the commonly used NDVI (normalized difference vegetation index) formula was applied to all pixels using the formula $(R_{750nm} - R_{705nm}) / (R_{750nm} + R_{705nm})$, and pixels with a value greater than 0.25 were classified as originating from the plant [13]. Second, based on the difference in reflectance between stem and leaves at wavelengths of 1056nm and 1151nm, the stem was segmented from other part of plants by selecting pixels where $(R_{1056nm} / R_{1151nm})$ produced a value greater than 1.2. Leaf pixels were defined as pixels identified as plant pixels based on NDVI but not classified as stem pixels. In addition to the biological variation between individual plants, overall intensity variation existed both between different plants imaged on the same day and the same plant on different days as a result of changes in the performance of the lighting used in the hyperspectral imaging chamber. To calibrate each individual image and make the results comparable, a python script (hosted on Github; see code availability section) was used to normalize the intensity values of each plant pixel using data from the non-plant pixels in the same image.

In order to visualize variation across 243 separate wavelength measurements across multiple plant images, we used a PCA (Principal Component Analysis) based approach. After the normalization described above, PCA analysis of intensity values for individual pixels was conducted. PCA values of each individual plant pixel per analyzed plant were translated to intensity values using the formula $[x - \min(x)] / [\max(x) - \min(x)]$. False color RGB images were constructed with the values for the first principal component stored in the red channel, the second principal component in the green channel and the third principal component stored in the blue channel.

Fluorescence Image Processing

A consistent area of interest was defined for each zoom level to exclude the pot and non-uniform areas of the imaging chamber backdrop. Within that area, pixels with an intensity value greater

1
2
3
4 270 than 70 in the red channel were considered to be plant pixels. The aggregate fluorescence
5 271 intensity was defined as the sum of the red channel intensity values for all pixels classified as
6 272 plant pixels within the region of interest, and the mean fluorescence intensity as the aggregate
7 273 fluorescence intensity value divided by the number of plant pixels within the region of interest.

274 275 **Plant Biomass Prediction**

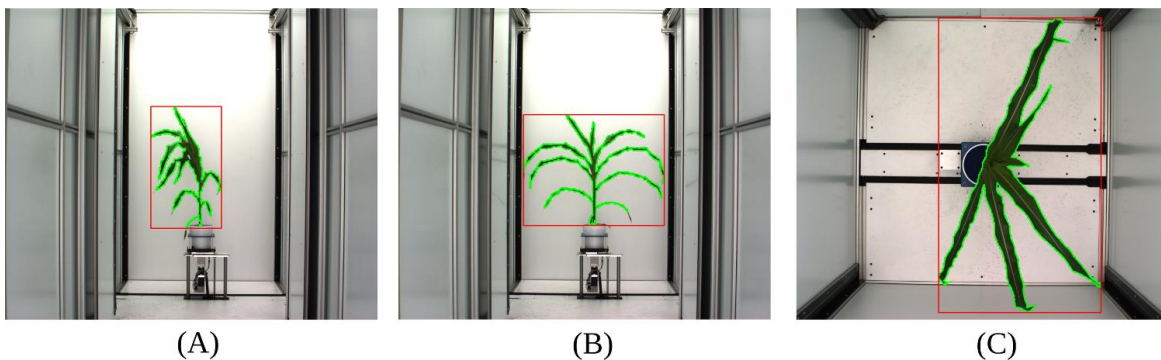
276
277 Two methods were used to predict plant biomass. The first was a single variable model based on
278 the number of zoom level adjusted plant pixels identified in the two RGB side view images on a
279 given day. The second was a multivariate model based upon the sum of plant pixels identified in
280 the two RGB side views, sum of plant pixels identified in the two RGB side views plus the RGB
281 top view, aggregate fluorescence intensity in the two side views, aggregate fluorescence intensity
282 in the two side views plus the top view, number of plant stem pixels identified in the
283 hyperspectral image and number of plant leaf pixels identified in the hyperspectral image. Traits
284 were selected to overlap with those employed by [14] where possible. This multivariate dataset
285 was used to predict plant biomass using linear modeling as well as MARS, Random Forest and
286 SVM [14]. MARS analysis was performed using the R package earth [15] Random Forest with the
287 R package randomForest [16] and SVM with the R package e1071 [17].

288 289 **Data Validation and Quality Control**

290 291 **Validation against ground truth measurements**

292
293 A total of approximately 500 GB of image data was initially generated by the system during the
294 course of this experiment consisting of RGB images (51.1%), fluorescence images (4.3%), and
295 hyperspectral images (44.6%). A subset of the RGB images within this dataset were previously
296 analyzed in [18], and were made available for download from <http://plantvision.unl.edu/dataset>
297 under the terms of the Toronto Agreement. To validate the dataset and ensure plants had been
298 properly tracked through both the automated imaging system and ground truth measurements, a
299 simple script was written to segment images into plant and not-plant pixels (Figure 1). Source
300 codes for all validation analysis are posted online

301 (https://github.com/shanwai1234/Maize_Phenoype_Map).



1
2
3
4
5 304
6 305 Figure 1: Segmentation of images into plant and not plant pixels for one representative plant (Path to this image in
7 306 the released dataset: Genotype_ZL019 -> Plant_008-19 -> Image_Type -> Day_32). The area enclosed by green
8 307 border is composed of pixels scored as "plant", the area outside the green border s composed of pixels scored as
9 308 "not-plant". Minimum bounding rectangle of plant pixels is shown in red. (A) Side view, angle 1; (B) Side view, 90
10 309 degree rotation relative to A; (C) Top View.
11 310
12

13 311 Based on the segmentation of the image into plant and non-plant pixels, plant height was scored
14 312 as the y axis dimension of the minimum bounding box. Plant area was scored as the total number
15 313 of plant pixels observed in both side view images after correcting for the area of each pixel at
16 314 each zoom employed (See Methods). Similar approaches to estimate plant biomass have been
17 315 widely employed across a range of grain crop species including ^[19], wheat ^[20], barley
18 316 ^[20,21],maize ^[12], sorghum ^[22] and seteria ^[9]. Calculated values were compared to manual
21 317 measurements of plant height and plant fresh biomass which were quantified using destructive
22 318 methods on the last day of the experiment. In both cases manual measurements and image
23 319 derived estimates were highly correlated, although the correlation between manual and estimated
24 320 height was greater than the correlation between manually measured and estimated biomass
25 321 (Figure 22A,B). Using the PlantCV software package ^[23], equivalent correlations between
27 322 estimated and ground truth biomass were obtained ($r=0.91$). Estimates of biomass using both
28 323 software packages were more correlated with each other ($r=0.96$) than either was with ground
29 324 truth measurements. This suggests that a significant fraction of the remaining error is the result
30 325 of the expected imperfect correlation between plant size and plant mass, rather than inaccuracies
31 326 in easimating plant size using individual software packages. Recent reports have suggested that
32 327 estimates of biomass incorporating multiple traits extracted from image data can increase
33 328 accuracy ^[14]. We tested the accuracy of biomass prediction of four multivariate estimation
34 329 techniques on this dataset (see Methods). The correlation coefficient (r value) of the estimated
35 330 biomass measures with ground truth data was 0.949, 0.958, 0.925 and 0.951 for multivariate
36 331 linear model, MARS, Random Forest and SVM respectively.
37
38
39

40 332
41 333 The residual value - difference between the destructively measured biomass value and the
42 334 predicted biomass value based on image data and the linear regression line equation – was
43 335 calculated for each individual plant (Figure 2C). Using data from the multiple replicates of each
44 336 individual accession, the proportion of error which is controlled by genetic factors rather than
45 337 random error can be ascertained. We determined that 58% of the total error in biomass estimate
46 338 was controlled by genetic variation between different maize lines. As such, this error is
47 339 systematic rather than random and thus more likely to produce misleading downstream results
48 340 when used in quantitative genetic analysis. As mentioned above, biomass and plant size are
49 341 imperfectly correlated, as different plants can exhibit different densities, for example as a result
50 342 of different leaf to stem ratios. Recent reports have suggested that estimates of biomass
51 343 incorporating multiple traits extracted from image data can increase accuracy ^[14]. We tested the
52 344 accuracy of biomass prediction of four multivariate estimation techniques on this dataset (see
53 345 Methods). The correlation of the estimated biomass measures with ground truth data was 0.949,
54 346 0.958, 0.925 and 0.951 for multivariate linear model, MARS, Random Forest and SVM
55 347 respectively. However, even when employing the most accurate of these four methods (MARS),
56 348 63% of the error in biomass estimation could be explained by genetic factors. This source of
57
58
59
60
61
62
63
64
65

error, with the biomass of some lines systematically underestimated and the biomass of other lines systematically overestimated presents a significant challenge to downstream quantitative genetic analysis. Given the prevalence of plant pixel counts as a proxy for biomass [20,22,9,21,12,19].

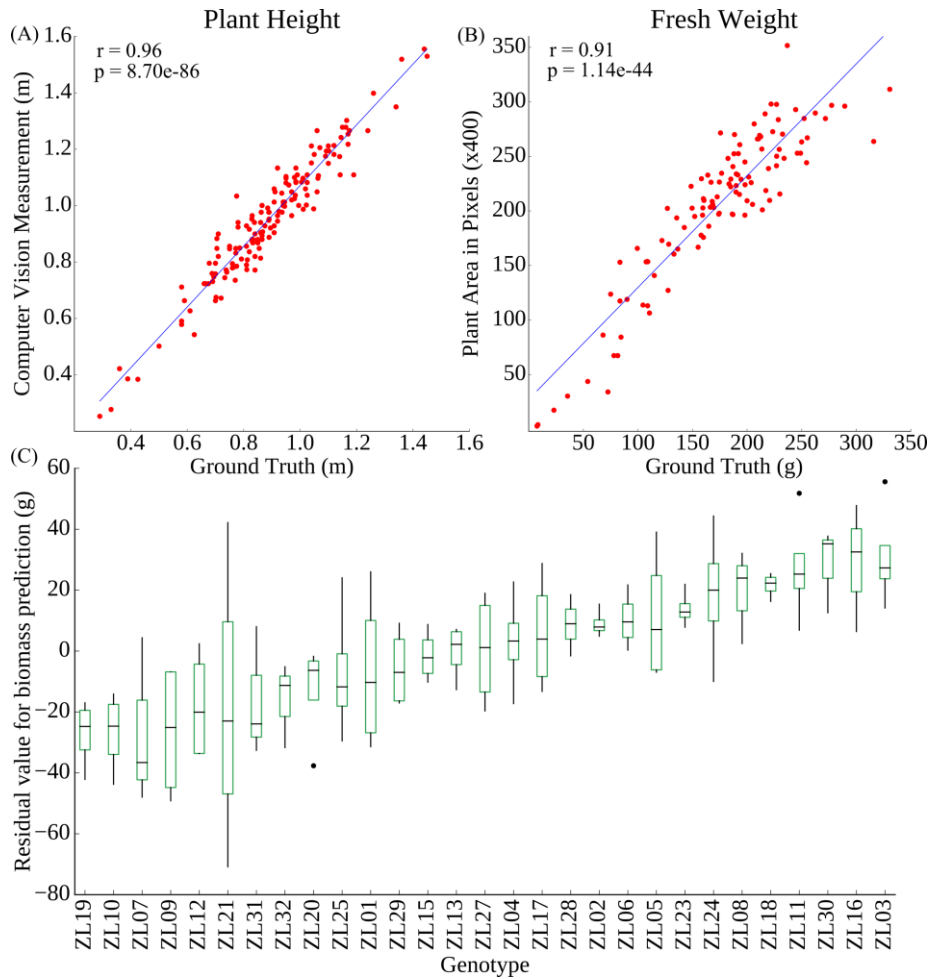


Figure 2: Correlation between image-based and manual measurements of individual plants. (A) Plant height; (B) Plant fresh biomass; (C) Variation in the residual between estimated biomass and ground truth measurement of biomass across inbreds.

Patterns of change over time

One of the desirable aspects of image based plant phenotyping is that, unlike destructively measured phenotypes, the same plant can be imaged repeatedly. Instead of providing a snapshot in time this allows researchers to quantify rates of change in phenotypic values over time, providing an additional set of derived trait values. Given the issues with biomass quantification presented above, measurements of plant height were selected to validate patterns of change in phenotypic values over time. As expected, height increases over time, and the patterns of increase tended to cluster together by genotype (Figure 3A). Increases in height followed by declines, as observed for ZL26, were determined to be caused by a change in the angle of the main stalk. While the accuracy of height estimates was assessed by comparison to physical ground truth measurements only on the last day, the height of three randomly selected plants

(Plant 007-26, Plant 002-7 and Plant 041-29) were manually measured from image data and compared to software based height estimates, and no significant differences were observed between the manual and automated measurements (Figure 3B; Supplementary Table 1). To perform a similar test of the accuracy of biomass estimation at different stages in the maize life cycle, a set of existing ground truth measurements for two genotypes under two stress treatments [12] were combined with additional later grow stage data (Supplemental Table 2). The correlation between total plant pixels observed in the two side views and plant biomass was actually substantially higher in this dataset ($r=0.97$) than the primary dataset, likely as a result of the smaller amount of genetic variability among these plants (Supplementary Figure 1).

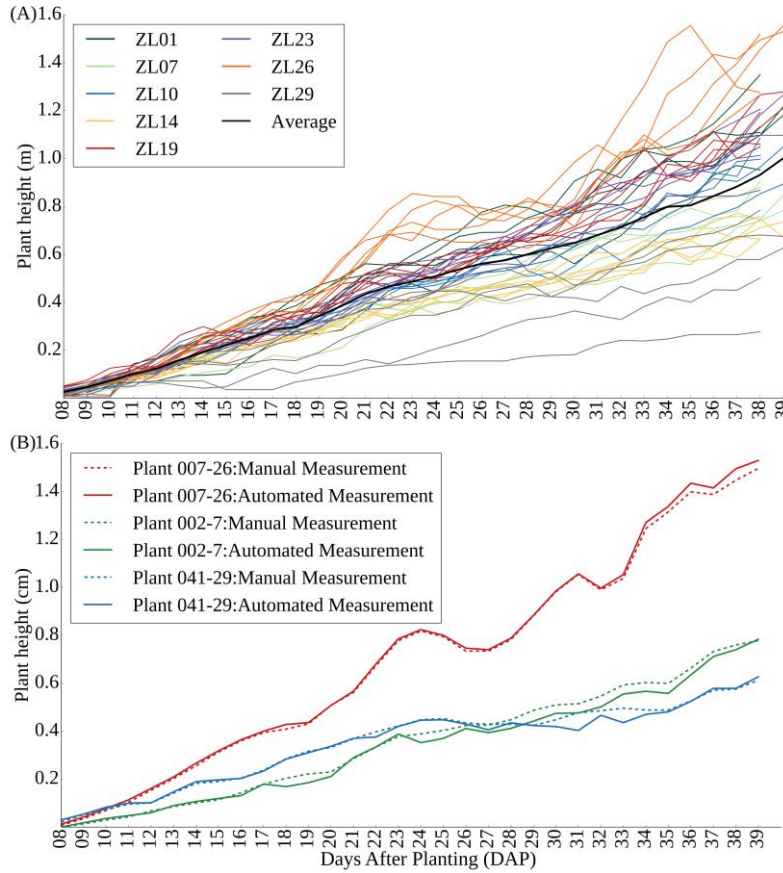


Figure 3: (A) Plant growth curves of each of five replicates of eight selected genotypes; (B) Comparison of manual measurements of plant height from image data with automated measurements for three randomly selected plants on each day of the experiment.

Heritability of phenotypes

The proportion of total phenotypic variation for a trait controlled by genetic variation is referred to as the heritability of that trait and is a good indicator of how easy or difficult it will be to either identify the genes which control variation in a given trait, or to breed new crop varieties in which a given trait is significantly altered. Broad-sense heritability can be estimated without the need to first link specific genes to variation in specific traits [24]. Variation in a trait which is not controlled by genotype can result from environmental effects, interactions between genotype and environment, random variance, and measurement error. Controlling for estimated row effects on

different phenotypic measurements significantly increased overall broad sense heritability (Figure 4A,B). This result suggests that even within controlled environments such as greenhouses, significant micro-environmental variation exists and that proper statistically based experimental design remains critical importance in even controlled environment phenotyping efforts.

If the absolute size of measurement error was constant in this experiment, as the measured values for a given trait became larger, the total proportion of variation explained by the error term should decrease and, as a result, heritability should increase as observed (Figure 4A). This trend was indeed observed across six different phenotypic measurements (three traits calculated from each of two viewing angles (Figure 4B). Plant height also exhibited significantly greater heritability than plant area or plant width and greater heritability when calculated solely from the 90 degree side angle photo than when calculated solely from to 0 degree angle photo.

In previous studies, fluorescence intensity has been treated as an indicator for plant abiotic stress status [25,26,7,27] or chlorophyll content level [28,29]. Using the fluorescence images collected as part of this experiment, the mean fluorescence intensity value for each plant image was calculated (see Methods). We found that this trait exhibited moderate heritability, with the proportion of variation controlled by genetic factors increasing over time and reaching approximately 60% by the last day of the experiment (Figure 4B).

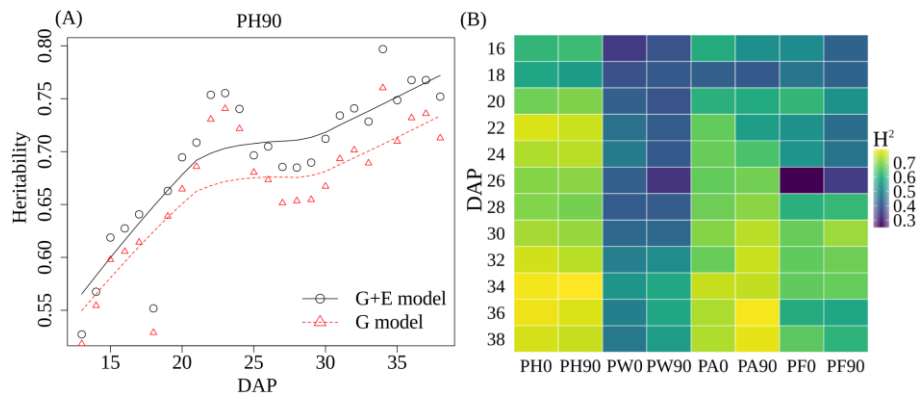


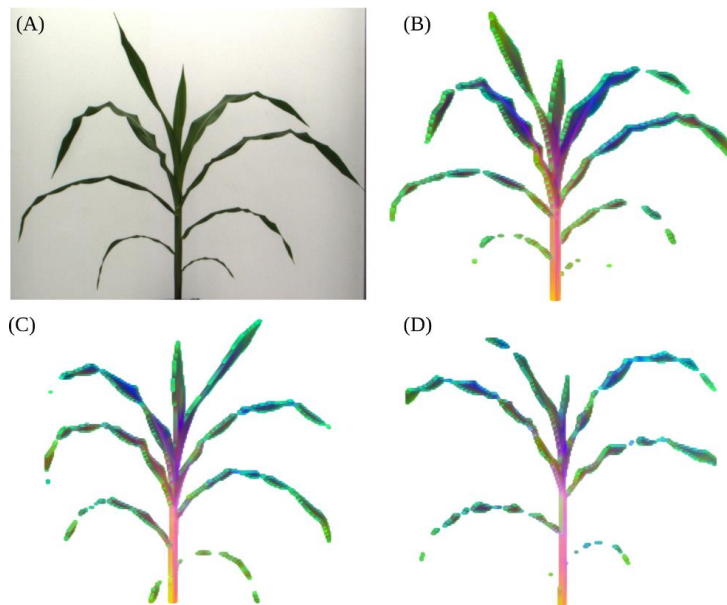
Figure 4: (A) The time course broad sense heritability of PH90. The heritability in the G model was calculated using a linear model that only considers the effect of genotype with residual values in the error term while heritability in the G+E model was calculated using a linear model that considers the effect of both genotype and environment (row effect) with residual values in the error term.; (B) The time course broad sense heritability of PA90 before and after controlling for the row effect; (B) Variation in broad-sense heritability (H^2) after controlling row effects for 6 trait measurements every second day across the phenotyping cycle. PA0: Plant Area in 0 degree (The major axis of leaf phylotaxy was parallel to the camera at 0 degree); PA90: Plant Area in 90 degree (The major axis of leaf phylotaxy was perpendicular to the camera at 90 degree); PH0: Plant Height in 0 degree; PH90: Plant Height in 90 degree; PW0: Plant Width in 0 degree; PW90: Plant Width in 90 degree; PF0: Average of plant fluorescence intensity in 0 degree; PF90: Average of plant fluorescence intensity in 90 degree.

Hyperspectral image validation

Hyperspectral imaging of crop plants has been employed previously in field settings using airborne cameras [30,31,32]. As a result of the architecture of grain crops such as maize, aerial

1
2
3
4 430 imagery will largely capture leaf tissue during vegetative growth, and either tassels (maize) or
5 431 seed heads (sorghum, millet, rice, oats, etc) during reproductive growth. The dataset described
6 432 here includes hyperspectral imagery taken from the side of individual plants, enabling
7 433 quantification of the reflectance properties of plant stems in addition to leaf tissue.

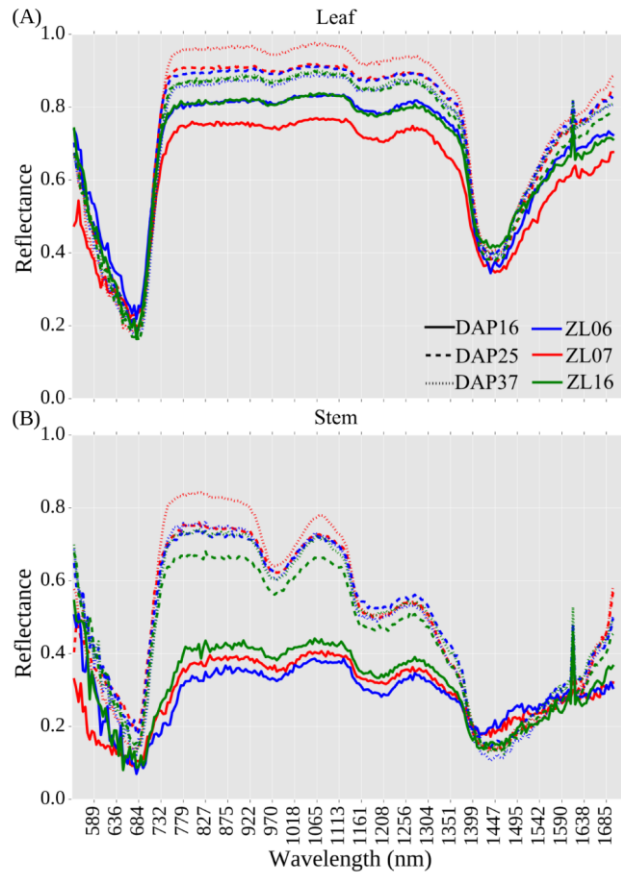
9 434 Many uses of hyperspectral data reduce the data from a whole plant or whole plot of
10 435 genetically identical plants to a single aggregate measurement. While these approaches can
11 436 increase the precision of intensity measurements for individual wavelengths, these approaches
12 437 also sacrifice spatial resolution and can in some cases produce apparent changes in reflectivity
13 438 between plants that result from variation in the ratios of the sizes of different organs with
14 439 different reflective properties. To assess the extent of variation in the reflectance properties of
15 440 individual plants, a principal component analysis of variation in intensity values for individual
16 441 pixels was conducted. After non-plant pixels were removed from the hyperspectral data cube
17 442 (Figure 5A) (See Methods), false color images were generated encoding the intensity values of
18 443 the first three principal components of variation as the intensity of the red, green, and blue
19 444 channels respectively (Figure 5B, C and D). The second principal component (green channel)
20 445 marked boundary pixels where intensity values likely represent a mixture of reflectance data
21 446 from the plant and from the background. The first principal component (red channel) appeared to
22 447 indicate distinctions between pixels within the stem of the plant and pixels within the leaves.
23
24
25
26
27 448



449
450 Figure 5: Segmentation and visualization of variation in hyperspectral signatures of representative maize plant
451 images. (A) RGB photo of Plant 013-2 (ZL02) collected on DAP 37; (B) False color image constructed of the same
452 corn plant from a hyperspectral photo taken on the same day. For each plant pixel the values for each of the first
453 three principal components of variation across 243 specific wavelength intensity values are encoded as one of the
454 three color channels in the false image; (C) Equivalent visualization for Plant 048-9 (ZL09); (D) Equivalent
455 visualization for Plant 008-19 (ZL19).
456

457 Based on this observation, an index was defined which accurately separated plant pixels into leaf
458 and stem (see Methods). Stem pixels were segmented from the rest of the plant using an index
459 value derived from the difference in intensity values observed in the 1056nm and 1151nm
460 hyperspectral bands. This methodology was previously described ^[12]. The reflectance pattern of
461 individual plant stems is quite dissimilar from the data observed from leaves and exhibits

1
 2
 3
 4 462 significantly different reflective properties in some areas of the near infrared (Figure 6).
 5 463 Characteristics of the stem are important breeding targets for both agronomic traits (lodging
 6 464 resistance, yield for biomass crops) and value added traits (biofuel conversion potential for
 7 465 bioenergy crops, yield for sugarcane and sweet sorghum). Hyperspectral imaging of the stem has
 8 466 the potential to provide nondestructive measurements of these traits. The calculated pattern of
 9 467 leaf reflectance for the data presented here are comparable with those observed in field-based
 10 468 hyperspectral studies ^[33,34,35], providing both external validation and suggesting that the data
 11 469 presented here may be of use in developing new indices for use under field conditions.
 12
 13
 14 470



15
 16
 17
 18
 19
 20
 21
 22
 23
 24
 25
 26
 27
 28
 29
 30
 31
 32
 33
 34
 35
 36
 37
 38
 39
 40
 41
 42
 43
 44 471
 45 472 Figure 6: Reflectance values for three plants - Plant 090-6 (ZL06), Plant 002-7 (ZL07), and Plant 145-16 (ZL16) on
 46 473 three days across development. (A) Reflectance values for non-stem plant pixels (i.e. leaves) (B) Reflectance values
 47 474 for pixels within the plant stem.
 48 475

49 476 In conclusion, while the results presented above highlight some of the simplest traits which can
 50 477 be extracted from plant image data, these represent a small fraction of the total set of phenotypes
 51 478 for which image analysis algorithms currently exist, and those in turn represent a small fraction
 52 479 of the total set of phenotypes which can potentially be scored from image data. Software
 53 480 packages already exist to measure a range of plant architectural traits such as leaf length, angle,
 54 481 and curvature from RGB images ^[6,36]. Tools are also being developed to extract phenotypic
 55 482 information on abiotic stress response patterns from fluorescence imaging ^[6,7]. The analysis of
 56 483 plant traits from hyperspectral image data, while common place in the remote sensing realm
 57 484 where an entire field may represent a single data point, is just beginning for single plant imaging.
 58 485 Recent work as highlighted the potential of hyperspectral imaging to quantify changes in plant
 59
 60
 61
 62
 63
 64
 65

1
2
3
4 486 composition and nutrient content throughout development ^[6,7]. While these techniques have great
5 487 potential to accelerate efforts to link genotype to phenotype through ameliorating the current
6 488 bottleneck of plant phenotypic data collection, it will be important to balance the development of
7 489 new image analysis tools with the awareness of the potential for systematic error resulting from
8 490 genetic variation between different lines of the same crop species.
9 491

11 492 **Availability of source code and requirements**

- 13 493
- 14 494 • Project name: Maize Phenotype Map
- 15 495 • Project home page: https://github.com/shanwai1234/Maize_Phenotype_Map
- 16 496 • Operating system(s): Linux
- 17 497 • Programming language: Python 2.7
- 18 498 • Other requirements: OpenCV module 2.4.8, Numpy >1.5, CMake > 2.6, GCC > 4.4.x,
- 19 499 Scipy 0.13
- 20 500 • License: BSD 3-Clause License
- 21 501

22 502 **Availability of supporting data and materials**

23 503

24 504 The image data sets from four types of cameras, pot weight records per day and ground truth
25 505 measurements with corresponding documentation for 32 maize inbreds and same types of image
26 506 data for two maize inbreds under two stress treatments were deposited in the CyVerse data
27 507 commons under a CC0 license with ^[38]. All image data were stored in the following data
28 508 structure: Genotype -> Plant -> Camera type -> Day. For the hyperspectral camera each photo is
29 509 stored as 243 sub images, each image representing intensity values for a given wavelength, so
30 510 these require one additional level of nesting in the data structure Day -> wavelength. The
31 511 grayscale images from the IR camera and the hyperspectral imaging system are stored as three-
32 512 channel images with all three channels in a given pixel set to identical values. The fluorescence
33 513 images contain almost all information in the red channel with the blue and green channel having
34 514 intensities equal to or very close to zero, but data all three channels exist. Genotype data of 32
35 515 inbreds were generated as part of a separate project and SNP calls for individual inbred lines
36 516 were made available either through ^[39] or the ZeaGBSv2.7 GBS SNP dataset stored in Panzea.
37 517 Measurements for thirteen core phenotypes at each field trial as well as local weather data can be
38 518 retrieved from publicly released Genomes 2 Fields datasets released on CyVerse ^[39,40]. Data from
39 519 the 2014 G2F field trials is posted ^[39] and data from the 2015 G2F field trials is posted ^[40].
40 520 Genetically identical seeds from the majority of the accessions used in creating both this dataset
41 521 and the Genomes 2 Fields field trial data can be ordered from public domain sources (e.g. USDA
42 522 GRIN) and are listed in Table 1. Further supporting metadata and snapshots of the Maize
43 523 Phenotype Map code are available in the GigaScience database, GigaDB ^[41].
44 524

45 525 **Declarations**

46 526 **List of abbreviations**

47 527

1
2
3
4 528 DAP: Days after planting
5 529 GBS: Genotyping by Sequencing
6 530 LED: Light-emitting diode
7 531 MARS: Multivariate Adaptive Regression Splines
8 532 NDVI: Normalized difference vegetation index
9 533 NIR: Near-infrared
10 534 RGB: An image with separate intensity values for the red, blue and green channels
11 535 SNP: Single Nucleotide Polymorphism
12 536 SVM: Support Vector Machines
13 537 UNL: University of Nebraska-Lincoln
14 538 PA0: Plant Area calculated from a 0 degree image. Plants were initially orientated then leaves
15 539 would be arranged parallel to the camera at 0 degrees.
16 540 PA90: Plant Area calculated from a 90 degree image. Plants were initially orientated then leaves
17 541 would be arranged perpendicular to the camera at 90 degrees.
18 542 PCA: Principal Component Analysis
19 543 PH0: Plant Height calculated from a 0 degree image
20 544 PH90: Plant Height calculated from a 90 degree image
21 545 PW0: Plant Width calculated from a 0 degree image
22 546 PW90: Plant Width calculated from a 90 degree image
23 547 PF0: Average of plant fluorescence intensity in 0 degree
24 548 PF90: Average of plant fluorescence intensity in 90 degree.
25
26
27
28
29
30
31

32 550 **Consent for publication**

33 551
34
35 552 Not applicable.
36 553
37

38 554 **Competing Interests**

39 555
40 556 The authors declare that they have no competing interests.
41
42
43

44 557 45 558 **Funding**

46 559
47 560 This research was supported by the Nebraska Corn Board (Award #88-R-1617-03), the Iowa
48 561 Corn Board (Award #), the National Science Foundation under Grant No. OIA-1557417, and
49 562 Internal University of Nebraska funding to JCS. The sources of funding have no role in the
50 563 design of the study and collection, analysis, and interpretation of data and in writing the
51 564 manuscript.
52
53
54
55

56 565 **Author's Contributions**

57 566
58
59
60
61
62
63
64
65

1
2
3
4
5
6
7
8
9
10
11
12
13
14
15
16
17
18
19
20
21
22
23
24
25
26
27
28
29
30
31
32
33
34
35
36
37
38
39
40
41
42
43
44
45
46
47
48
49
50
51
52
53
54
55
56
57
58
59
60
61
62
63
64
65

JCS, and YQ designed the experiment; VS, JCS and ZL performed data acquisition; ZL, PP, YQ, YX, YG and JCS analyzed and interpreted the data; ZL and JCS produced and curated the metadata; ZL and JCS implemented software; ZL and JCS prepared the initial draft. All authors reviewed the manuscript.

Acknowledgements

The authors are grateful to Yang Zhang, Xianjun Lai and Daniel WC Ngu for help in collecting manual measurements of plants, Thomas Hoban for manually counting pixels of selected plant images, Kent M. Eskridge for valuable discussions on experimental design, Addie Thompson, Jinliang Yang for assistance on heritability analysis, and the members of the Genomes 2 Fields consortium for sharing both seed and datasets prior to publication. CyVerse is supported by the U.S. National Science Foundation under award numbers DBI-0735191 and DBI-1265383.

References

1. Grassini P, Eskridge KM, Cassman KG. Distinguishing between yield advances and yield plateaus in historical crop production trends. *Nature communications* 2013;4:2918.
2. Hartmann A, Czauderna T, Ho mann R, Stein N, Schreiber F. HTPPheno: an image analysis pipeline for high-throughput plant phenotyping. *BMC bioinformatics* 2011;12(1):148.
3. Topp CN, Iyer-Pascuzzi AS, Anderson JT, Lee CR, Zurek PR, Symonova O, et al. 3D phenotyping and quantitative trait locus mapping identify core regions of the rice genome controlling root architecture. *Proceedings of the National Academy of Sciences* 2013;110(18):E1695-E1704.
4. Das A, Schneider H, Burrige J, Ascanio AKM, Wojciechowski T, Topp CN, et al. Digital imaging of root traits (DIRT): a high-throughput computing and collaboration platform for field-based root phenomics. *Plant methods* 2015;11(1):51.
5. Zhang X, Huang C, Wu D, Qiao F, Li W, Duan L, et al. High-throughput phenotyping and QTL mapping reveals the genetic architecture of maize plant growth. *Plant physiology* 2017;p. pp-01516.
6. Chen D, Neumann K, Friedel S, Kilian B, Chen M, Alt- mann T, et al. Dissecting the phenotypic components of crop plant growth and drought responses based on high-throughput image analysis. *The Plant Cell* 2014;26(12):4636-4655.
7. Campbell MT, Knecht AC, Berger B, Brien CJ, Wang D, Walia H. Integrating image-based phenomics and association analysis to dissect the genetic architecture of temporal salinity responses in rice. *Plant physiology* 2015;168(4):1476-1489.

- 1
2
3
4 601 8. Munns R, James RA, Sirault XR, Furbank RT, Jones HG. New phenotyping methods for
5 602 screening wheat and barley for beneficial responses to water deficit. *Journal of experimental*
6 603 *botany* 2010;61(13):3499-3507.
8
9 604 9. Fahlgren N, Feldman M, Gehan MA, Wilson MS, Shyu C, Bryant DW, et al. A versatile
10 605 phenotyping system and analytics platform reveals diverse temporal responses to water
11 606 availability in *Setaria*. *Molecular plant* 2015;8(10):1520-1535.
13
14 607 10. Lobet G, Draye X, Périlleux C. An online database for plant image analysis software tools.
15 608 *Plant methods* 2013;9(1):38.
17
18 609 11. Campbell D, de Leon N, Edwards J, Gardiner J, Al Khalifah N, Lawrence-Dill C, et al.
19 610 *Genomes to Fields* 2016 data release. *CyVerse Data Commons* 2016.
21
22 611 12. Ge Y, Bai G, Stoerger V, Schnable JC. Temporal dynamics of maize plant growth, water use,
23 612 and leaf water content using automated high throughput RGB and hyperspectral imaging.
24 613 *Computers and Electronics in Agriculture* 2016;127:625-632.
25
26 614 13. Gamon J, Surfus J. Assessing leaf pigment content and activity with a reflectometer. *New*
27 615 *Phytologist* 1999;143(1):105-117.
29
30 616 14. Chen D, Shi R, Pape JM, Klukas C. Predicting plant biomass accumulation from image-
31 617 derived parameters. *bioRxiv* 2016;p. 046656.
33
34 618 15. Milborrow S. *Earth: multivariate adaptive regression spline models*. R package version
35 619 2014;3:2-7.
36
37 620 16. Liaw A, Wiener M, et al. *Classification and regression by randomForest*. R news
38 621 2002;2(3):18-22.
40
41 622 17. Dimitriadou E, Hornik K, Leisch F, Meyer D, Weingessel A. *Misc Functions of the*
42 623 *Department of Statistics (e1071)*, TU Wien. R package version 2005;p. 1-5.
44
45 624 18. Choudhury SD, Stoerger V, Samal A, Schnable JC, Liang Z, Yu JG. *Automated Vegetative*
46 625 *Stage Phenotyping Analysis of Maize Plants using Visible Light Images*. *Data Science for Food,*
47 626 *Energy and Water workshop*, San Francisco, California, USA, August 2016.
49
50 627 19. Al-Tamimi N, Brien C, Oakey H, Berger B, Saade S, Ho YS, et al. *Salinity tolerance loci*
51 628 *revealed in rice using high-throughput non-invasive phenotyping*. *Nature communications*
52 629 2016;7.
54
55 630 20. Golzarian MR, Frick RA, Rajendran K, Berger B, Roy S, Tester M, et al. *Accurate inference*
56 631 *of shoot biomass from high-throughput images of cereal plants*. *Plant methods* 2011;7(1):2.
58
59
60
61
62
63
64
65

1
2
3
4
5
6
7
8
9
10
11
12
13
14
15
16
17
18
19
20
21
22
23
24
25
26
27
28
29
30
31
32
33
34
35
36
37
38
39
40
41
42
43
44
45
46
47
48
49
50
51
52
53
54
55
56
57
58
59
60
61
62
63
64
65

21. Honsdorf N, March TJ, Berger B, Tester M, Pillen K. High-throughput phenotyping to detect drought tolerance QTL in wild barley introgression lines. *PLoS one* 2014;9(5):e97047.

22. Neilson EH, Edwards A, Blomstedt C, Berger B, Møller BL, Gleadow R. Utilization of a high-throughput shoot imaging system to examine the dynamic phenotypic responses of a C4 cereal crop plant to nitrogen and water deficiency over time. *Journal of experimental botany* 2015;66(7):1817-1832.

23. Gehan MA, Fahlgren N, Abbasi A, Berry JC, Callen ST, Chavez L, et al. PlantCV v2. 0: Image analysis software for high-throughput plant phenotyping. *PeerJ Preprints*; 2017.

24. Holland JB, Nyquist WE, Cervantes-Martínez CT. Estimating and interpreting heritability for plant breeding: an update. *Plant breeding reviews* 2003;22:9-112.

25. VanKooten O, Snel JF. The use of chlorophyll fluorescence nomenclature in plant stress physiology. *Photosynthesis research* 1990;25(3):147-150.

26. Fracheboud Y, Haldimann P, Leipner J, Stamp P. Chlorophyll fluorescence as a selection tool for cold tolerance of photosynthesis in maize (*Zea mays* L.). *Journal of experimental botany* 1999;50(338):1533-1540.

27. Kalaji HM, Jajoo A, Oukarroum A, Brestic M, Zivcak M, Samborska IA, et al. Chlorophyll a fluorescence as a tool to monitor physiological status of plants under abiotic stress conditions. *Acta Physiologiae Plantarum* 2016;38(4):102.

28. Murchie EH, Lawson T. Chlorophyll fluorescence analysis: a guide to good practice and understanding some new applications. *Journal of experimental botany* 2013;64(13):3983-3998.

29. Guanter L, Zhang Y, Jung M, Joiner J, Voigt M, Berry JA, et al. Global and time-resolved monitoring of crop photosynthesis with chlorophyll fluorescence. *Proceedings of the National Academy of Sciences* 2014;111(14):E1327-E1333.

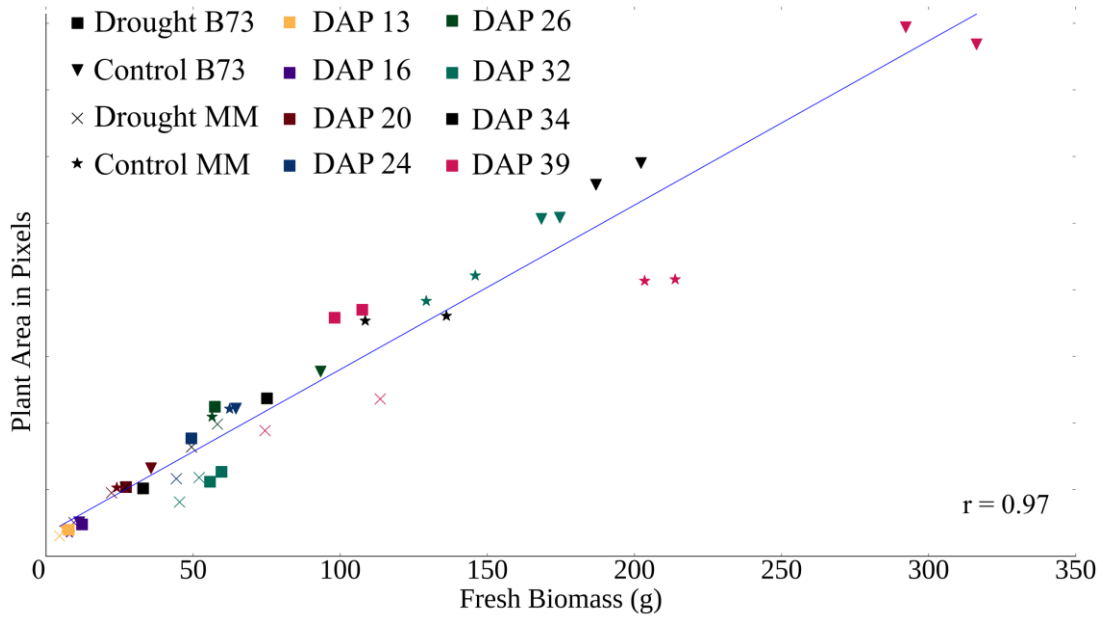
30. Zarco-Tejada P, Catalina A, González M, Martín P. Relationships between net photosynthesis and steady-state chlorophyll fluorescence retrieved from airborne hyperspectral imagery. *Remote Sensing of Environment* 2013;136:247-258.

31. Zaman-Allah M, Vergara O, Araus J, Tarekegne A, Magorokosho C, Zarco-Tejada P, et al. Unmanned aerial platform-based multi-spectral imaging for field phenotyping of maize. *Plant methods* 2015;11(1):35.

32. Yendrek C, Tomaz T, Montes CM, Cao Y, Morse AM, Brown PJ, et al. High-throughput phenotyping of maize leaf physiology and biochemistry using hyperspectral reflectance. *Plant physiology* 2016;p. pp-01447.

- 1
2
3
4 664 33. Smith K, Steven M, Colls J. Use of hyperspectral derivative ratios in the red-edge region to
5 665 identify plant stress responses to gas leaks. *Remote sensing of environment* 2004;92(2):207-217.
6
7
8 666 34. Zhao D, Reddy KR, Kakani VG, Reddy V. Nitrogen deficiency effects on plant growth, leaf
9 667 photosynthesis, and hyperspectral reflectance properties of sorghum. *European Journal of*
10 668 *Agronomy* 2005;22(4):391-403.
11
12
13 669 35. Baranowski P, Jedryczka M, Mazurek W, Babula- Skowronska D, Siedliska A, Kaczmarek J.
14 670 Hyperspectral and thermal imaging of oilseed rape (*Brassica napus*) response to fungal species of
15 671 the genus *Alternaria*. *PloS one* 2015;10(3):e0122913.
16
17
18 672 36. Klukas C, Chen D, Pape JM. Integrated analysis platform: an open-source information
19 673 system for high-throughput plant phenotyping. *Plant physiology* 2014;165(2):506-518.
20
21 674 37. Pandey P, Ge Y, Stoerger V, Schnable JC. High throughput in vivo analysis of plant leaf
22 675 chemical properties using hyperspectral imaging. *Frontiers in Plant Science* 2017;8.
23
24
25 676 38. Maize Image Phenotype Dataset Released in Association with this paper.
26 677 <https://doi.org/10.7946/P22K7V>.
27
28
29 678 39. Publicly Released Genomes 2 Fields 2014 Field Trial Dataset.
30 679 <https://doi.org/10.7946/P2V888>.
31
32
33 680 40. Publicly Released Genomes 2 Fields 2015 Field Trial Dataset.
34 681 <https://doi.org/10.7946/P24S31>.
35
36 682 41. Liang Z, Pandey P, Stoerger V, Xu Y, Qiu Y, Ge Y, et al. Supporting data for “Conventional
37 683 and hyperspectral time-series imaging of maize lines widely used in field trials”. *GigaScience*
38 684 *Database* 2017; <http://dx.doi.org/10.5524/100371>.
39
40

41 685 **Supplementary Information**
42
43
44
45
46
47
48
49
50
51
52
53
54
55
56
57
58
59
60
61
62
63
64
65



686

687

688

689

Figure S1. Correlation of fresh weight biomass with total number of plant pixels identified in two side view images for maize plants destructively sampled at eight different time points between 13 days and 39 days after planting (DAP).

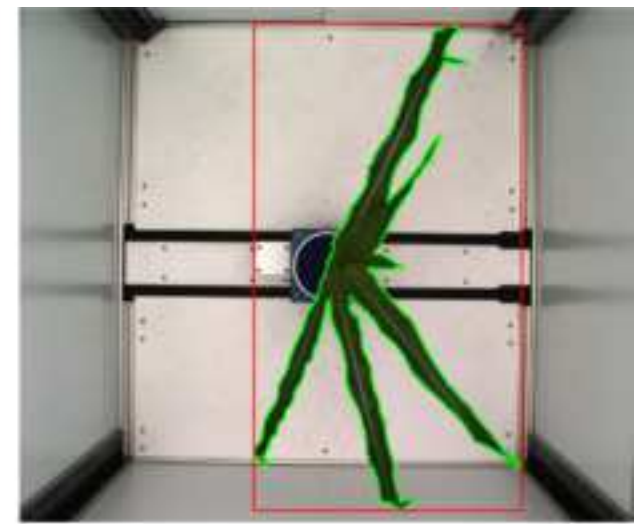
1
2
3
4
5
6
7
8
9
10
11
12
13
14
15
16
17
18
19
20
21
22
23
24
25
26
27
28
29
30
31
32
33
34
35
36
37
38
39
40
41
42
43
44
45
46
47
48
49
50
51
52
53
54
55
56
57
58
59
60
61
62
63
64
65



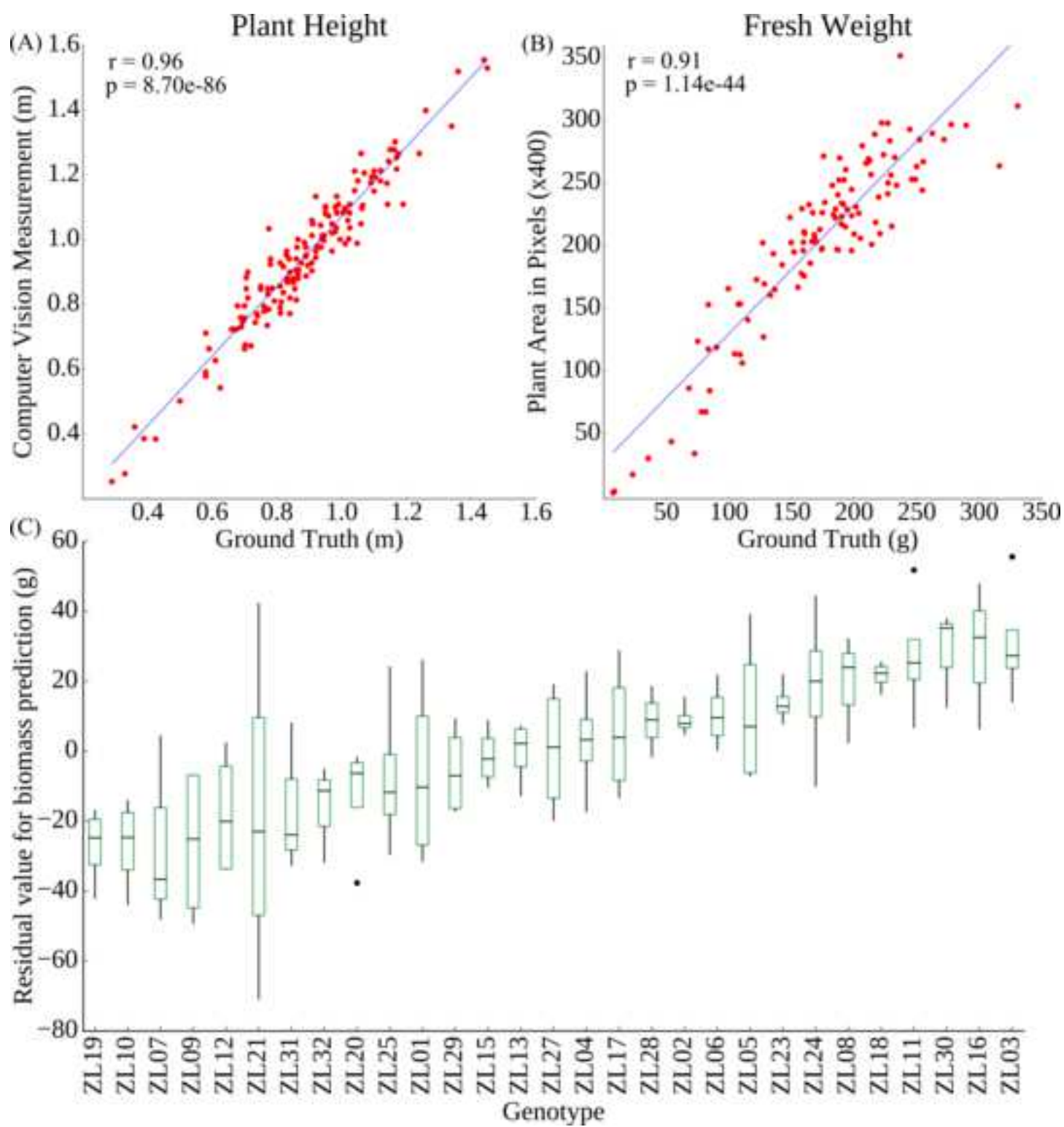
(A)

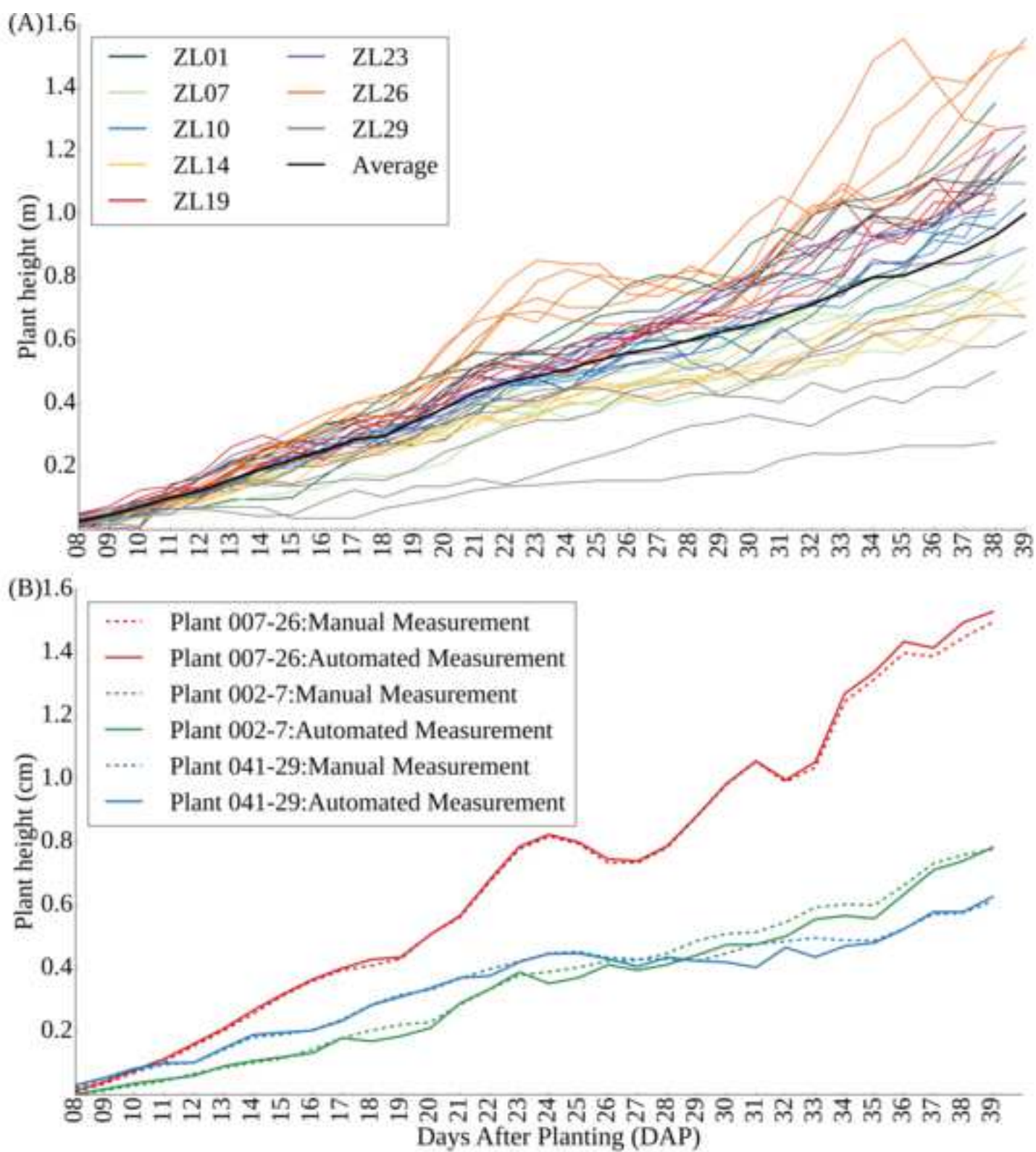


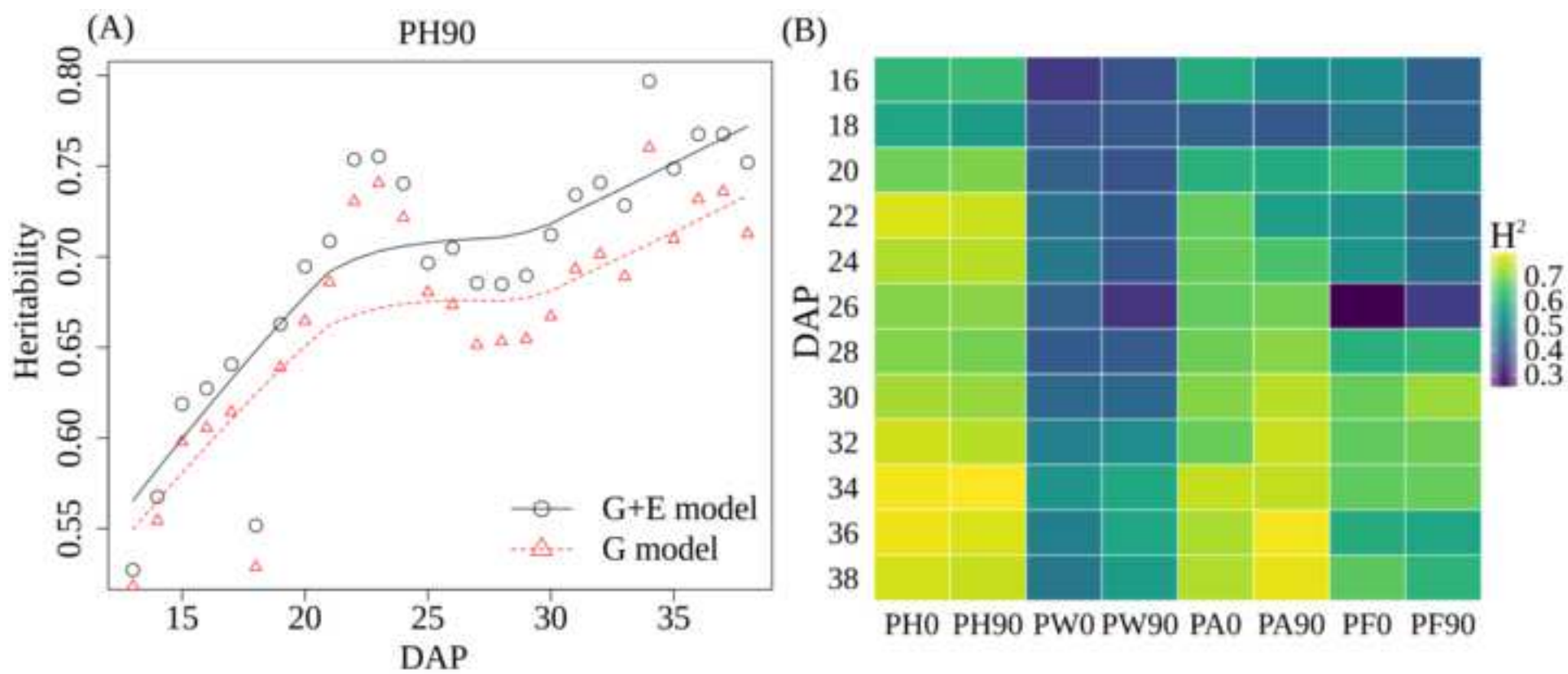
(B)

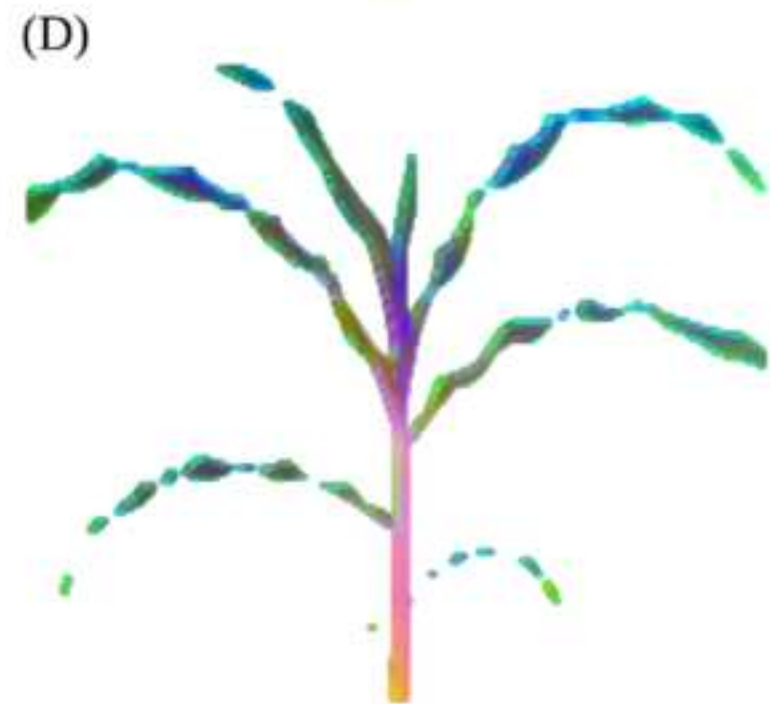
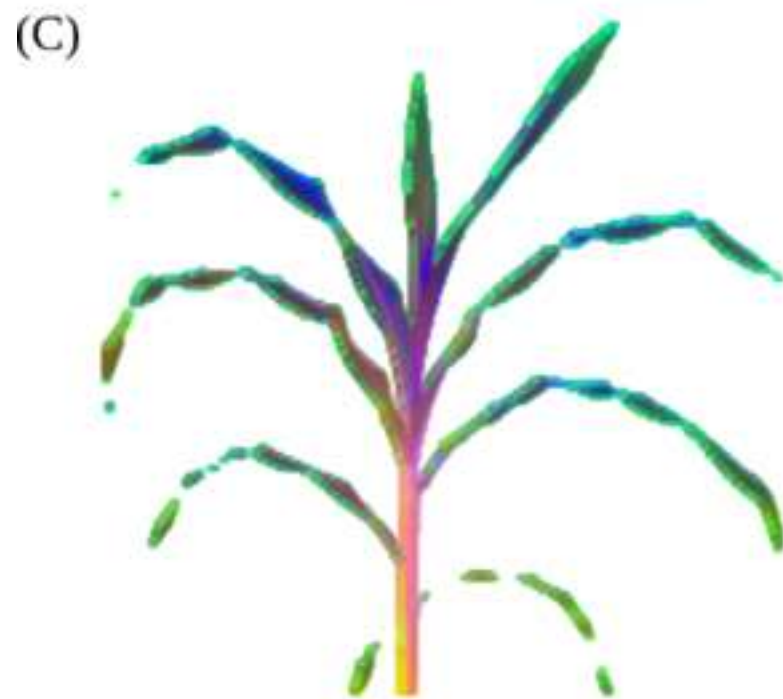
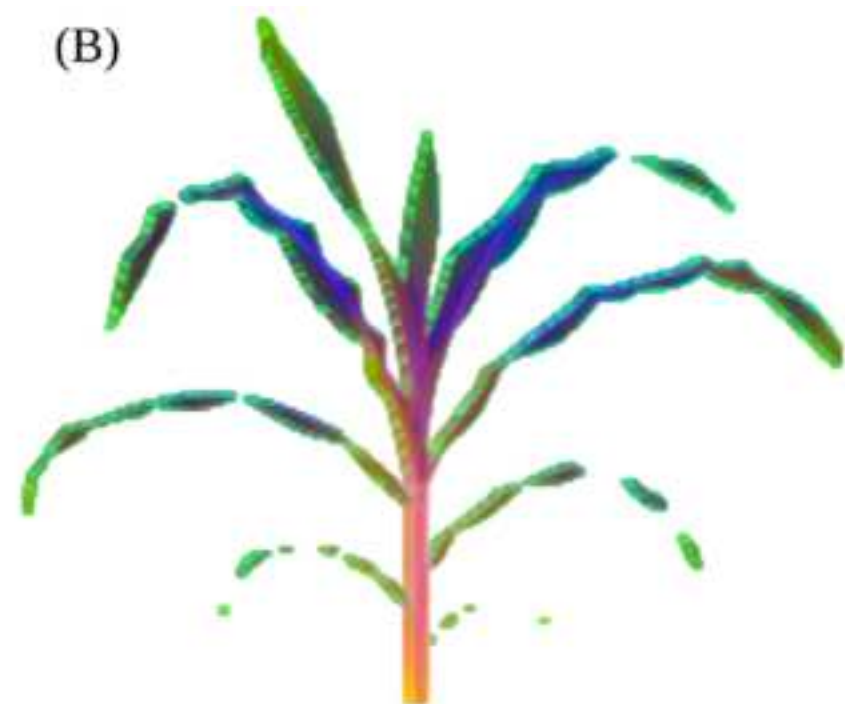


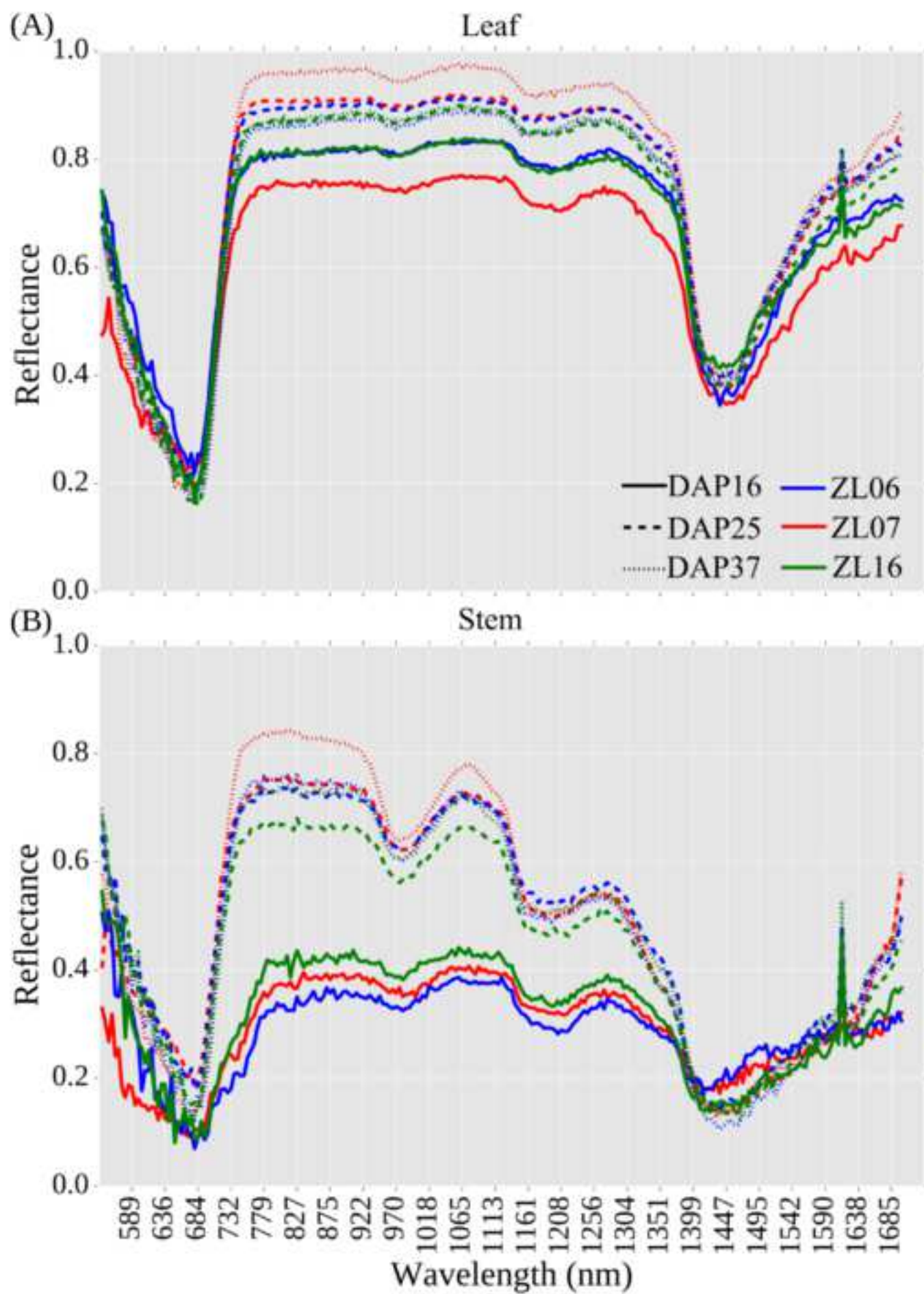
(C)







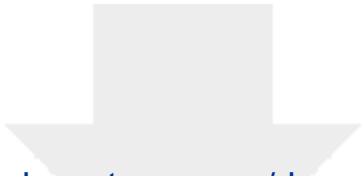




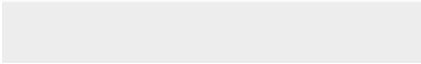



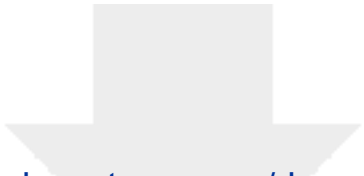
Click here to access/download
Supplementary Material
gigascience-logo.pdf



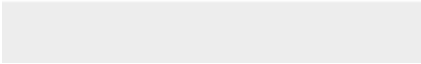



Click here to access/download
Supplementary Material
main.bbl





Click here to access/download
Supplementary Material
main.tex





Click here to access/download
Supplementary Material
oup-contemporary.cls





Click here to access/download
Supplementary Material
oup.pdf





Click here to access/download
Supplementary Material
paper-refs.bib





Click here to access/download
Supplementary Material
Supplementary_Figure_1.png



Click here to access/download
Supplementary Material
vancouver-authoryear.bst

